doi:10.1006/jmbi.2000.3722 available online at http://www.idealibrary.com on IDEAL® J. Mol. Biol. (2000) 299, 255–279

JMB

Hydrogen Bonding and Catalysis: A Novel Explanation for How a Single Amino Acid Substitution Can Change the pH Optimum of a Glycosidase

Manish D. Joshi[1], Gary Sidhu[1], Isabelle Pot[1], Gary D. Brayer[1] Stephen G. Withers[1,2] and Lawrence P. McIntosh[1,2]*

[1]*The Department of Biochemistry and Molecular Biology and the Protein Engineering Network of Centres of Excellence University of British Columbia Vancouver, BC, Canada V6T 1Z3*

[2]*The Department of Chemistry University of British Columbia Vancouver, BC, Canada V6T 1Z1*

**Corresponding author*

The pH optima of family 11 xylanases are well correlated with the nature of the residue adjacent to the acid/base catalyst. In xylanases that function optimally under acidic conditions, this residue is aspartic acid, whereas it is asparagine in those that function under more alkaline conditions. Previous studies of wild-type (WT) *Bacillus circulans* xylanase (BCX), with an asparagine residue at position 35, demonstrated that its pH-dependent activity follows the ionization states of the nucleophile Glu78 (pK_a 4.6) and the acid/base catalyst Glu172 (pK_a 6.7). As predicted from sequence comparisons, substitution of this asparagine residue with an aspartic acid residue (N35D BCX) shifts its pH optimum from 5.7 to 4.6, with an ~20 % increase in activity. The bell-shaped pH-activity profile of this mutant enzyme follows apparent pK_a values of 3.5 and 5.8. Based on ^{13}C-NMR titrations, the predominant pK_a values of its active-site carboxyl groups are 3.7 (Asp35), 5.7 (Glu78) and 8.4 (Glu172). Thus, in contrast to the WT enzyme, the pH-activity profile of N35D BCX appears to be set by Asp35 and Glu78. Mutational, kinetic, and structural studies of N35D BCX, both in its native and covalently modified 2-fluoro-xylobiosyl glycosyl-enzyme intermediate states, reveal that the xylanase still follows a double-displacement mechanism with Glu78 serving as the nucleophile. We therefore propose that Asp35 and Glu172 function together as the general acid/base catalyst, and that N35D BCX exhibits a ''reverse protonation'' mechanism in which it is catalytically active when Asp35, with the lower pK_a, is protonated, while Glu78, with the higher pK_a, is deprotonated. This implies that the mutant enzyme must have an inherent catalytic efficiency at least 100-fold higher than that of the parental WT, because only ~1 % of its population is in the correct ionization state for catalysis at its pH optimum. The increased efficiency of N35D BCX, and by inference all ''acidic'' family 11 xylanases, is attributed to the formation of a short (2.7 Å) hydrogen bond between Asp35 and Glu172, observed in the crystal structure of the glycosyl-enzyme intermediate of this enzyme, that will substantially stabilize the transition state for glycosyl transfer. Such a mechanism may be much more commonly employed than is generally realized, necessitating careful analysis of the pH-dependence of enzymatic catalysis.

Keywords: pH-dependent enzyme mechanism; NMR; X-ray crystallography; isotope shift; electrostatics

Present address: I. Pot, The Centre for Molecular Medicine and Therapeutics (CMMT), University of British Columbia, Vancouver, BC, Canada, V5Z 4H4.

Abbreviations used: WT, wild-type; BCX, *Bacillus circulans* xylanase; ESMS, electrospray mass spectrometry; $ONPX_2$, orthonitrophenyl β-xylobioside; δΔ, the magnitude and direction of the chemical shift change upon deprotonation of the listed residue; pH*, the measured pH without correction for isotope effect; $2,5\text{-}DNPX_2$, 2,5-dinitrophenyl β-xylobioside; DNP2FXb, 2,4-dinitrophenyl 2-deoxy-2-fluoro-β-xylobioside; 2FXb, 2-fluoro-2-β-xylobioside; β_{lg}, Brønsted coefficient for general acid/base catalysis; $3,4\text{-}DNPX_2$, 3,4-dinitrophenyl β-xylobioside; PhX_2, phenyl β-xylobioside; LBHB, low barrier hydrogen bond; CGTase, cyclodextrin glycosyl transferase; PPA, pig pancreatic α-amylase; HPA, human pancreatic α-amylase.

E-mail address of the corresponding author: mcintosh@otter.biochem.ubc.ca

0022-2836/00/010255–25 $35.00/0

Introduction

Enzymes catalyze biological reactions using a variety of ionizable groups functioning as electrophiles, nucleophiles, or general acid/base catalysts. As a result, the pH-dependent activity of an enzyme is set primarily by the pK_a values of one or a few key ionizable groups within its active-site cleft. A long-standing challenge is to define experimentally and theoretically the factors that establish the precise pK_a values of these catalytically essential groups along a given reaction pathway and thereby set the conditions of pH under which an enzyme is maximally active. A better understanding of these factors will also aid in the engineering of enzymes with tailored pH optima.

The low molecular mass xylanases (Gilkes *et al*., 1991) provide a fascinating example of how the pH-dependence of enzymatic catalysis can be modulated within a family of retaining glycosidases. Members of endo-β-(1,4)-glycosidase family 11 (or G) derive from both eukaryotic and bacterial species and share sequence identity varying from 40-90 % (Torronen *et al*., 1993; Torronen & Rouvinen, 1997). All members of this family studied to date have strikingly similar three-dimensional structures and active-site geometries (Torronen & Rouvinen, 1997). In particular, they all contain two catalytically essential glutamic acid residues that are involved in an intricate network of hydrogen bonds contributed by highly conserved neighboring residues (Torronen & Rouvinen, 1997; Wakarchuk *et al*., 1994). One catalytic glutamic acid residue functions as a nucleophile and the other as a general acid/base catalyst in a double-displacement mechanism whereby hydrolysis of xylosidic substrates proceeds with retention of anomeric configuration (Gebler *et al*., 1992; Koshland, 1953; Sinnot, 1990). In spite of all these similarities, the pH optima of family 11 xylanases vary widely from acidic values as low as 2 to alkaline values as high as 11 (see Table 6).

A comparison of the sequences of these low molecular mass endo-β-(1,4)-glycosidases reveals a striking correlation, in that the residue hydrogen bonded to the general acid/base catalyst is asparagine in so-called ''alkaline'' xylanases, whereas it is aspartic acid in those with a more ''acidic'' pH optimum (Torronen & Rouvinen, 1997). This seems counter-intuitive, since it might be expected that placement of a negatively charged residue next to the acid/base catalyst should electrostatically elevate its pK_a and raise the pH optimum of the enzyme to a more alkaline value. Nevertheless, this correlation has been confirmed by mutational analysis of *Aspergillus kawachii* xylanase C, in which the single substitution of Asn for Asp at this key position dramatically elevates its pH optimum from ~2 to 5 (Fushinobu *et al*., 1998). Several studies of these family 11 xylanases have led to proposed mechanisms by which this paradoxical effect may be manifest (Fushinobu *et al*., 1998; Krengel & Dijkstra, 1996), though none of these explanations has been entirely satisfactory.

In order to understand how the substitution of a single amino acid residue can modulate the pH optimum of an enzyme, we have focused our attention on the ''alkaline'' xylanase from *Bacillus circulans* (BCX) (Sung *et al*., 1993; Wakarchuk *et al*., 1992). This 20.4 kDa protein has been characterized extensively using a wide range of structural, spectroscopic, and enzymatic techniques, and is thus an excellent model system for investigating the factors that establish the pH-dependence of the activity of a retaining glycosidase (Birsan *et al*., 1998; Lawson *et al*., 1996, 1997; McIntosh *et al*., 1996; Miao *et al*., 1994; Sidhu *et al*., 1999). The active site of BCX is composed of several highly conserved residues arranged to form an intricate network of hydrogen bonds surrounding two catalytically essential acidic residues, Glu78 and Glu172 (Wakarchuk *et al*., 1994). Previous studies have determined that Glu78 functions as the nucleophile, while Glu172 is the general acid/base catalyst (McIntosh *et al*., 1996; Miao *et al*., 1994; Sidhu *et al*., 1999). The NMR spectrum of BCX has been assigned (Plesniak *et al*., 1996b) and the pK_a values of all of the carboxyl (Joshi *et al*., 1997; McIntosh *et al*., 1996) and imidazole (Plesniak *et al*., 1996a) groups have been determined. Specifically, the pK_a values of Glu78 and Glu172, measured directly using ^{13}C-NMR spectroscopy, are 4.6 and 6.7, respectively. These values are in close agreement with those determined from the bell-shaped pH-activity profile of this enzyme and thereby provide a straightforward explanation for its observed pH optimum near 5.7 (McIntosh *et al*., 1996).

In this study, we have substituted the asparagine residue (Asn35), adjacent to the general acid/base catalyst Glu172 in BCX, with an aspartic acid residue. As predicted by sequence comparisons, this substitution led to a pronounced decrease in the pH optimum of the enyzme to 4.6. We have thoroughly investigated this phenomenon, combining kinetic studies using synthetic aryl β-xylobioside substrates, site-specific measurements of the pK_a values of catalytic groups by ^{13}C-NMR spectroscopy, electrospray mass spectrometry (ESMS), and X-ray crystallographic structure determination. Integrating these analyses, we propose a detailed mechanism to explain the dependence of the pH optima of family 11 xylanases on the nature of the group adjacent (Asn or Asp) to the acid/base catalyst.

Results

pH-dependent activity of N35D BCX

Comparison of the pH-dependence of the second-order rate constant, k_{cat}/K_m, for the hydrolysis of orthonitrophenyl β-xylobioside ($ONPX_2$) by WT and N35D BCX reveals that the point mutation causes a pronounced shift in the pH optimum of this enzyme from 5.7 to 4.6 and an

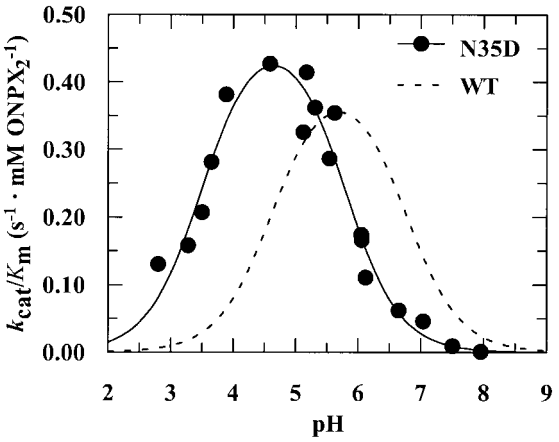

Figure 1. pH-dependence of k_{cat}/K_m for N35D BCX (●) at 25 °C towards the synthetic substrate orthonitrophenyl β-xylobioside ($ONPX_2$). Substitution of an Asp residue at position 35 shifts the pH optimum from 5.7 for the WT protein to 4.6 for the N35D mutant. The activity profile follows ionizations with pK_a values of 3.5 and 5.8 in the N35D enzyme (—) and 4.6 and 6.7 in the WT enzyme (---) (McIntosh *et al.*, 1996). The data points, shown only for N35D BCX, were fitted as described in Materials and Methods.

increase in its activity by ~20 % (Figure 1). Therefore, a single substitution at position 35 leads to a decrease in pH optimum by 1.1 units. This is consistent with previous studies of family 11 xylanases where there is Asp at position 35 for those with an ''acidic'' pH optimum, and Asn for those functioning with an ''alkaline'' pH optimum (Fushinobu *et al.*, 1998; Krengel & Dijkstra, 1996; Torronen & Rouvinen, 1995).

The activity profile of N35D BCX is characterized by an acidic limb that follows an apparent pK_a of 3.5 and a basic limb that follows a pK_a of 5.8 when fitted to a model involving two ionizable sites. This is noticeably different from the pH-dependent activity of WT BCX, whose profile is characterized by two ionizations with apparent pK_a values of 4.6 and 6.7 for the acidic and basic limbs, respectively. Previous studies of WT BCX have shown that the group that ionizes with a pK_a of 4.6 is the nucleophile Glu78, while that with a pK_a of 6.7 is the general acid catalyst Glu172 (McIntosh *et al.*, 1996; Miao *et al.*, 1994; Wakarchuk *et al.*, 1994). Extrapolation to N35D BCX would lead to the erroneous prediction that Glu78 has a pK_a of 3.5 and Glu172 has a pK_a of 5.8 in this mutant protein (discussed later). However, on the basis of the structure, this is counter-intuitive. The presence of Asp35 might be expected to either not change (in the case of a neutral aspartic acid residue), or to elevate (a negatively charged aspartic acid residue) the pK_a of the neighboring Glu172, relative to that found in the WT protein with Asn35, and thus shift the pH optimum to a more basic rather than to a more acidic value.

Structure of N35D BCX

The crystal structure of N35D BCX was determined at pH 7.5 to a resolution of 1.55 Å with an *R*-factor of 19.4 % (Tables 1 and 2; Figure 2). This structure is highly similar to that of WT BCX (Wakarchuk *et al.*, 1994), with an overall r.m.s. deviation of only 0.23 Å for all atoms between these two models. Upon detailed inspection, it is seen that the side-chain of Asp35 adopts approximately the same conformation as that of the WT Asn35, differing only in the χ_2 dihedral angle by a rotation of ~16 °. A small rotation in χ_3 (~8 °) of Glu172 is also observed. Correspondingly, the distance between Asn35 $N^{\delta 2}$/Asp35 $O^{\delta 2}$ and Glu172 $O^{\varepsilon 2}$ increases very slightly from 3.1 Å in WT BCX to 3.2 Å in N35D BCX due to the amino acid substitution at position 35 (Table 3) (note, as shown below, at pH 7.5, Asp35 is negatively charged and Glu172 is neutral in N35D BCX, whereas in the WT protein, Asn35 is neutral and Glu172 is negatively charged). Asp35 $O^{\delta 2}$ in the variant structure also forms an additional, albeit bent, hydrogen bond with the amide nitrogen atom of Phe36 (bond angle $O^{\delta 2} \cdots HN = 120\,^{\circ}$). This interaction is not possible in the WT enzyme, as Asn35 $N^{\delta 2}$ and Phe36 N are unable to hydrogen bond to one another. The exchange of asparagine for aspartate at position 35 appears to increase the thermal motion of both residues 35 and 172, as determined from normalized isotropic thermal factors. The average thermal factor for residue 35 increases from 11 Å^2 to 17 Å^2, while for residue 172 this parameter increases from 11 Å^2 to 14 Å^2. No significant change in the position of Glu78 is observed. The only other noteworthy perturbations are small (~0.5-0.7 Å) shifts in the positions of the guanido groups of Arg112, which is within the binding cleft of BCX, and Arg122, which is exposed on the surface of protein. In summary, only subtle structural perturbations accompany the substitution of Asp for Asn35. Thus, there is no apparent conformational basis for the shift in pH optimum of

Table 1. X-ray crystallographic data collection parameters

Parameters	N35D BCX	N35D-2FXb BCX
Space group	$P2_12_12_1$	$P2_12_12_1$
Cell dimensions (Å)		
a	44.05	43.83
b	52.69	52.74
c	78.61	78.80
Number of measurements	150,984	99,311
Number of unique reflections	27,301	17,579
Mean $I/\sigma I$	21.1 (7.0)	25.8 (11.1)
Merging *R*-factor (%)[a,b]	5.7 (15.2)	5.7 (14.2)
Resolution range (Å)	∞-1.55	∞-1.8

[a] Values in parentheses are for data in the highest resolution shell (1.61-1.55 Å for N35D BCX and 1.86-1.80 Åfor N35D-2FXb BCX).

[b] $R_{merge} = \Sigma_{hkl}\ \Sigma_{i=0}^{n} |I_i - I_{hkl}| / \Sigma_{hkl}\ \Sigma_{i=0}^{n} I_{i_{hkl}}$.

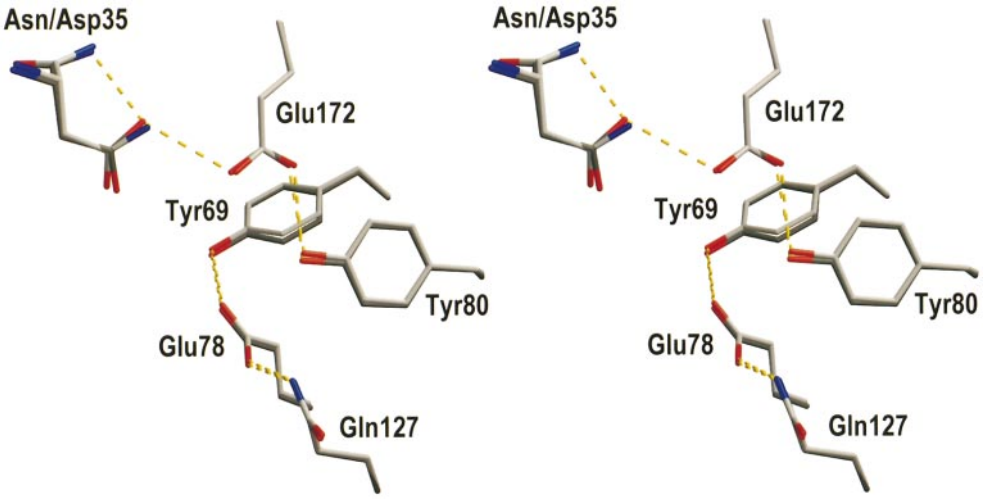

Figure 2. A stereo-drawing of the structural conformations of key active-site residues of N35D BCX (dark gray) superimposed upon those of WT BCX residues (light gray) (pH 7.5). Potential hydrogen bonds are indicated by broken yellow lines, oxygen atoms are shown in red and nitrogen atoms in blue. The structures are highly similar with an overall r.m.s deviation of only 0.23 Å. See Table 3 for a listing of selected interatomic distances.

N35D BCX to a more acidic value compared to the WT enzyme.

Direct measurement of the pK_a values of the catalytic residues of N35D BCX

To ascertain which groups are responsible for the activity profile of N35D BCX, the pK_a values of the catalytic residues were measured directly by monitoring the pH-dependence of the carbonyl ^{13}C-NMR chemical shifts of the Glu and Gln side-chains. Analysis of the titration curves of [δ-^{13}C]glutamic acid-labelled N35D BCX protein shows a noteworthy difference when compared to WT BCX (McIntosh *et al*., 1996) (Figure 3). That is, the titration curves of Glu78 and Glu172 are triphasic instead of biphasic, indicating the presence of an additional ionizable group in the active site. As discussed later, this third titrating group is assigned as Asp35.

The biphasic nature of the titration curves measured previously for Glu78 and Glu172 in WT BCX has been attributed to electrostatic and/or structural coupling of the ionization equilibria of these two catalytic residues. As discussed in detail by Shrager *et al*. (1972), two or more ionizable groups may show coupled or biphasic titration curves if either the microscopic pK_a or the chemical shift of one is dependent upon the ionization state of the other. The first case is analogous to the classic branched equilibria of a dibasic acid in which each carboxyl group has two microscopic pK_a values, corresponding to the neutral and charged states of its interacting partner. The second case reflects the fact that the chemical shifts of one residue may be dependent upon the ionization state of the second, for example, through electric field effects or structural perturbations. (An example of this case is when the chemical shift of a non-ionizable group is dependent upon the protonation states of nearby titratable groups). Fitting of the titration data for WT BCX to either model reveals that the predominant pK_a values of Glu78 and Glu172 are 4.6 and 6.7, respectively. These arguments hold for triphasic titration curves involving three coupled protonatable groups. However, with eight possible ionization states, the data cannot be readily fit to extract the desired microscopic pK_a values (see Scheme 1 and Discussion). We therefore chose to fit the titration curves measured for N35D BCX to simple equations describing sequential ionization equilibria in order to extract apparent pK_a values. We attribute the apparent pK_a value corresponding to the largest positive chemical shift change (ionized *versus* neutral) of each Glu or Asp residue to reflect its own ionization, and those cor-

Table 2. X-ray crystallographic refinement statistics

Parameters	N35D-BCX	N35D-2FXb BCX
Number of reflections	25,023	16,559
Resolution range (Å)	10-1.55	10-1.8
Completeness within range (%)	91.8	94.5
Number of non-hydrogen protein atoms	1448	1448
Number of non-hydrogen ligand atoms		18
Number of solvent atoms	146	129
Average thermal factors (Å^2)		
Protein	13.2	12.3
Ligand		23.2
Solvent	36.6	34.0
Final refinement *R*-factor (%)[a]	19.4	19.3
Stereochemistry	r.m.s. deviations	
Bonds (Å)	0.007	0.007
Angles (deg.)	1.210	1.136

[a] $R\text{-factor} = \Sigma_{hkl}|F_{o,hkl} - F_{c,hkl}| / \Sigma_{hkl}|F_{o,hkl}|$.

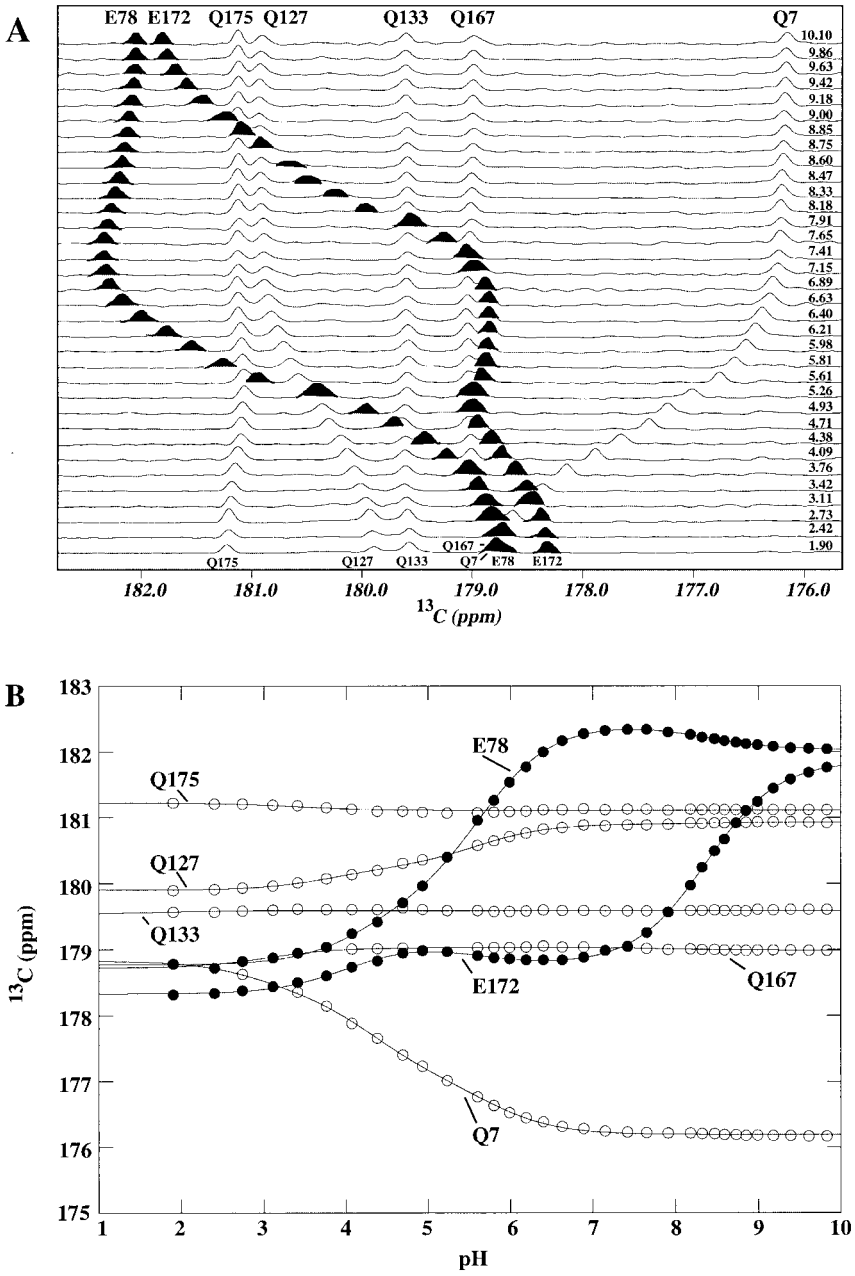

Figure 3. (a) ^{13}C-NMR spectra of N35D BCX recorded as a function of pH at 25 °C. The peaks corresponding to Glu78 and Glu172 are shaded in black for emphasis. Spectral assignments were based on previous analysis of WT BCX (McIntosh *et al.*, 1996) and pH values are listed above each spectrum. (b) Apparent pK_a values were determined by fitting the data for the two Glu (●) and five Gln (○) carbonyl groups to an equation describing the pH-dependence of the chemical shift of a residue to one or more sequential ionization events.

responding to smaller chemical shift changes to the ionization equilibria of neighboring residues.

In the case of N35D BCX, the titration curve of Glu78 has three apparent pK_a values (Table 4). The first, with a minor chemical shift change of +0.96 ppm, follows a macroscopic pK_a of 4.2 and is attributed to the ionization of Asp35. The second, with a major chemical shift change of +2.69 ppm, follows a pK_a of 5.7 and is assigned to the ionization of Glu78 itself. Finally, a third, with a minor chemical shift change of −0.39 ppm, follows a pK_a of 8.4 and reflects the ionization of Glu172. Similarly, in the titration curve of Glu172, three apparent pK_a values can be observed. The first minor chemical shift change of +0.76 ppm follows a pK_a of 4.0 and is due to the ionization of Asp35. The second minor chemical shift change of −0.32 ppm follows a pK_a of 5.5 and is due to the ionization of Glu78. Finally, a third and major chemical shift change of +3.09 ppm follows a pK_a of 8.4 and is assigned to the ionization of Glu172 itself. In a similar manner, the ionization of Asp35 was monitored directly in a [γ-^{13}C]Asp-labelled N35D protein (data not shown). The titration curve of Asp35

Table 3. Selected interatomic distances within the active-site of WT and N35D BCX

Interaction	Distances (Å)			
	N35D	N35D-2FXb	WT[a]	WT-2FXb[a]
Asn/Asp35 $N^{\delta2}/O^{\delta2}$-Glu172 $O^{\varepsilon2}$	3.2	2.7	3.1	3.3
Glu78 $O^{\varepsilon2}$-Asn/Asp35 $O^{\delta1}$	6.6	6.2	6.4	6.5
Glu78 $O^{\varepsilon2}$-Glu172 $O^{\varepsilon2}$	5.6	5.5	5.6	5.8
Asn/Asp35 $N^{\delta2}/O^{\delta2}$-Phe36 N	2.9	2.9	3.2	3.0
Glu172 $O^{\varepsilon2}$-Wat[b]	3.7	3.9	3.8	3.1
Glu172 $O^{\varepsilon1}$-Tyr80 O^{η}	2.9	2.9	2.7	2.8
Tyr80 O^{η}-Wat[b]	2.9	2.8	2.8	2.7
Glu78 $O^{\varepsilon2}$-Tyr69 O^{η}	2.5	2.9	2.6	3.0
Glu78 $O^{\varepsilon2}$-Gln127 $N^{\varepsilon2}$	2.7	2.6	2.7	2.6
Glu172 $O^{\varepsilon2}$-Arg112 N^{ε}	7.0	7.2	7.1	7.2
Asn/Asp35 $N^{\delta2}/O^{\delta2}$-Asp11 $O^{\delta2}$	6.1	5.9	6.1	6.0
Glu78 $O^{\varepsilon2}$-Arg112 N^{ε}	5.9	5.9	6.2	6.0
Asn/Asp35 $N^{\delta2}/O^{\delta2}$-Arg112 N^{ε}	8.1	7.9	7.8	7.9

[a] Structural coordinates used for distance measurements were obtained from the RCSB Protein Data Bank, PDB identification number 1XNB for WT BCX (Wakarchuk *et al*., 1994) and 1BVV for WT-2FXb BCX (Sidhu *et al*., 1999).
[b] See Figure 5 and the text for a discussion.

is biphasic in nature and reflects two pK_a values: the first major chemical shift change of +2.13 ppm follows a pK_a of 3.7 and is attributed to the ionization of Asp35 itself, whereas the second minor change in chemical shift of +1.07 ppm follows a pK_a of 5.6 and is due to the ionization of Glu78. The pK_a of Glu172 was not apparent in the titration curve of Asp35 because the data used to directly measure the pK_a of Asp35 did not extend beyond pH 8.3.

The resonances of the side-chain δ carbonyl groups of all Gln residues are detected in the ^{13}C-NMR spectra of N35D BCX (Figure 3). Their presence is due to the metabolic interconversion of glutamic acid to glutamine in *Escherichia coli*. The ^{13}C chemical shifts of the non-ionizable Gln residues are pH-dependent due to the influence of other titratable side-chains within the protein; thus these serve as reporter groups to further verify the pK_a values measured for residues 35, 78 and 172. In particular, in N35D BCX the pH-dependent chemical shift of Gln7 predominantly follows two pK_a values; namely, a pK_a of 3.9 ($\delta\Delta = 1.37$ ppm) due to the ionization of Asp35, and a pK_a of 5.6 ($\delta\Delta = 1.17$ ppm) due to the ionization of Glu78. In the WT protein, the resonance of Gln7 follows the titrations of Glu78 (pK_a 4.5, $\delta\Delta = 2.09$ ppm) and Glu172 (pK_a 6.5, $\delta\Delta = 0.47$ ppm) (McIntosh *et al*., 1996). Similarly, the resonance of Gln127 is pH-dependent, following the ionizations of Glu172

Table 4. Experimentally measured apparent pK_a values of N35D and WT BCX obtained from ^{13}C-NMR pH titrations

Residue	N35D BCX		WT BCX[c]	
	pK_a	δΔ[a] (ppm)	pK_a	δΔ[a] (ppm)
Glu78	4.2	+0.96	<u>4.6</u>	+2.80
	<u>5.7</u>	+2.69	6.5	+0.33
	8.4	−0.39		
Glu172	4.0	+0.76	<u>6.7</u>	+2.78
	5.5	−0.32	4.6	+0.44
	<u>8.4</u>	+3.09		
Asp35	<u>3.7</u>	+2.13		
	5.6	+1.07		
	N35D-2FXb BCX		WT-2FXb BCX[b]	
Glu78-2FXb	(2.9[e])	−0.03	[d]	[d]
	(9.3[e])	−0.18		
Glu172	1.9[e]	+1.63	<u>4.2</u>	+1.58
	3.4[e]	+0.48		
	9.0	+0.10		

The major apparent pK_a, assigned to the ionization of the given residue, is underlined. An error in the pK_a value of ±0.1 pH unit is estimated from the error in pH measurements.
[a] The δΔ value refers to the magnitude and direction of the chemical shift change upon deprotonation of the listed residue. The error in chemical shift is estimated to be ±0.015 ppm.
[b] Data taken from McIntosh *et al*. (1996).
[c] Change in chemical shift does not reflect ionization of the residue itself, since it is covalently attached to the inhibitor.
[d] No observable pH-dependent change in chemical shift.
[e] See the text for a discussion.

(pK_a 8.4, $\delta\Delta = 0.03$ ppm), Glu78 (pK_a 5.6, $\delta\Delta = 0.65$ ppm) and Asp35 (pK_a 3.8, $\delta\Delta = 0.65$ ppm) in N35D BCX and of Glu172 (pK_a 6.6, $\delta\Delta = 0.32$ ppm) and Glu78 (pK_a 4.5, $\delta\Delta = 0.76$ ppm) in the WT protein (McIntosh *et al*., 1996).

The analyses of the ionization behavior of Asp35, Glu78 and Glu172 are further supported by deuterium isotope shift measurements (Joshi *et al*., 1997; Ladner *et al*., 1975; Yamazaki *et al*., 1994). An estimate of the protonation state of a carboxyl group can be made by observing the difference in its ^{13}C chemical shift in H_2O *versus* ^2H_2O solutions. A neutral carboxylic acid group is expected to show an isotope shift of ~ -0.25 ppm between its protonated and deuterated forms, whereas a carboxylate group would show no such effect. Measurement of the deuterium isotope shift of the δ side-chain carbon atoms of Glu78 and Glu172 in N35D BCX protein reveals that at pH* 6.32, Glu78 is deprotonated (no apparent isotope shift), whereas Glu172 is protonated (isotope shift of −0.29 ppm). These data are consistent with the measured pK_a values of the three active-site carboxyl groups in N35D BCX.

Based on both titration curves and isotope shifts, we conclude that the pK_a values corresponding primarily to the ionizations of Asp35, Glu78 and Glu172 in N35D BCX are 3.7, 5.7 and 8.4, respectively. The small differences in the corresponding pK_a values measured from the multiphasic titration curves of the Asp, Glu and Gln residues (Table 4) are attributed to difficulties in accurately fitting these data and the complex nature of the structural or electrostatic interactions in this highly coupled network of ionizable side-chains. Regardless, these data clearly differ from the pK_a values of 4.6 and 6.8 measured for Glu78 and Glu172 in the WT enzyme, and confirm the expectation that the substitution of Asn35 by Asp elevates the pK_a values of the nearby catalytic glutamic acid residues.

Determining the catalytic roles of Asp35, Glu78 and Glu172

The directly measured pK_a values of Asp35, Glu78, and Glu172 indicate that the pH-dependent activity of N35D BCX appears to follow the ionization of Asp35 (pK_a 3.7) and Glu78 (pK_a 5.7). The pK_a of Glu172 (8.4) is not apparent in the activity profile. This presents an interesting problem, as the acidic limb of the activity profile, which reflects the deprotonation of the nucleophile Glu78 in WT BCX, now appears to follow the ionization of Asp35, while the basic limb of the activity profile, which reflects the need to have the acid catalyst Glu172 protonated in WT BCX, now appears to follow the ionization of Glu78. These observations begged the question of whether the mechanism of BCX had changed due to the substitution of Asn35 by Asp.

To address this question, several experimental approaches were utilized. First, determination of the stereochemical course of hydrolysis using 2,5-$DNPX_2$ as a substrate indicated that, as with the WT enzyme, the initial product released was the β anomer of the xylobiose (Figure 4). Hence, both WT and N35D BCX utilize a double-displacement retaining mechanism to hydrolyze aryl β-xylobiosides.

Second, the role of Glu78 as the nucleophile was ascertained by three methods. The essential function of Glu78 was confirmed by the observation that the N35D/E78Q double mutant has no detectable activity on $ONPX_2$ (Table 5). Similarly, the single (nucleophile) mutant E78Q BCX is completely inactive. Using electrospray mass spectrometry (ESMS), we demonstrated that a mechanism-based inhibitor, 2,4-dinitrophenyl 2-deoxy-2-fluoro-β-xylobioside (DNP2FXb), covalently attaches to Glu78. In particular, tryptic digestion of inhibited N35D BCX yielded the same doubly charged,

Table 5. Steady-state kinetic parameters for the hydrolysis of aryl β-xylobiosides for N35D and WT BCX

Phenol substituent	pK_a[a]	Protein	k_{cat}[b] (s^{-1})	K_m[b] (mM)	k_{cat}/K_m[b] (s^{-1} mM^{-1})
2,5-Dinitro	5.15	**N35D**	**14.8**	**6.7**	**2.6**
(2,5-$DNPX_2$)		WT[c]	76	2.2	35
3,4-Dinitro	5.36	**N35D**	**8.2**	**48.1**	**0.18**
(3,4-$DNPX_2$)		WT[c]	8.3	3.4	2.7
2-Nitro	7.22	**N35D**	**14.5**	**25.6**	**0.56**
($ONPX_2$)		WT[d]	9.6	14	0.66
		N35D/E172Q	0.72	33.3	0.021
		E172Q[e]	0.62	8.3	0.075
		N35D/E78Q	[f]	[f]	[f]
		E78Q	[f]	[f]	[f]
Unsubstituted	9.99	**N35D**	**0.14**	**20.1**	**0.0070**
(PhX_2)		WT[e]	0.051	8.7	0.0050

Assays were carried out at pH 6.0 and 40 °C.

[a] Phenol pK_a values were taken from Tull & Withers (1994).

[b] Values of k_{cat}/K_m were taken from the slope of the Lineweaver-Burk plot, whereas values of k_{cat} and K_m were determined from a non-linear fit of the Michaelis-Menten equation.

[c] Data taken from Ziser *et al*. (1995).

[d] Data taken from Lawson *et al*. (1996).

[e] Data taken from Lawson *et al*. (1997).

[f] No detectable enzymatic hydrolysis (unpublished results).

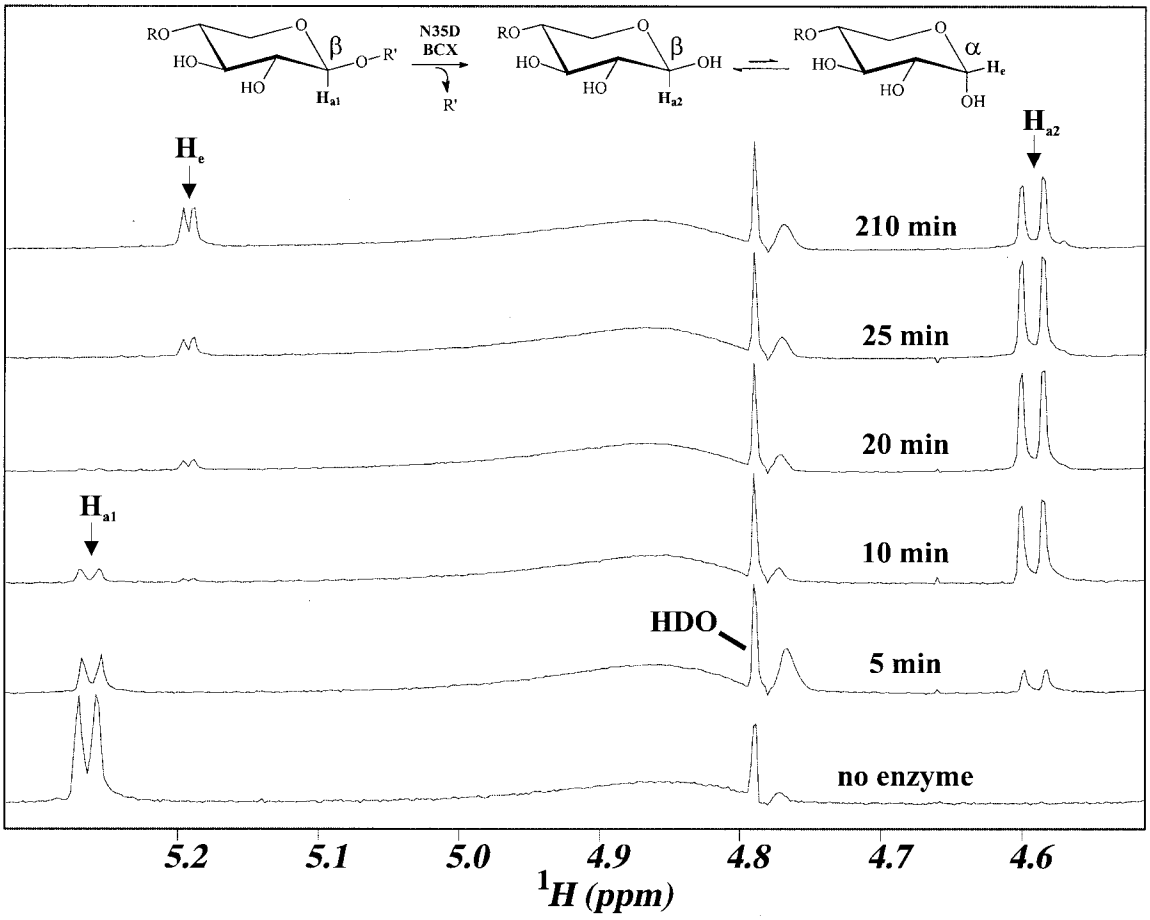

Figure 4. Stereochemical course of hydrolysis of $ONPX_2$ by N35D BCX at 25 °C, 99.9 % ^2H_2O and pH* 4.8. ^{1}H-NMR spectra were recorded as a function of time after addition of $ONPX_2$ substrate (R = xylose, R′ = 2′ dinitrophenyl). The control spectrum of $ONPX_2$ with no enzyme (bottom) shows a doublet at 5.26 ppm ($J = 7.0$ Hz) corresponding to the axial anomeric proton of the xylose residue nearest to the aryl leaving group (R′), H_{a1}, that is present in the β-anomer of the unhydrolyzed substrate. Initially ($t <$ ten minutes) after the addition of N35D enzyme, the doublet at 5.26 ppm disappears while a new doublet at 4.59 ppm ($J = 7.9$ Hz) appears. This is due to the axial proton, H_{a2}, of the initial β-anomeric product released and demonstrates that the mechanism of N35D BCX involves stereochemical retention of anomeric configuration of the product. As time proceeds ($t =$ 20-210 minutes) mutarotation of the initial product occurs, as is evident by the appearance of a second peak at 5.19 ppm ($J = 3.5$ H_z) due to the presence of the α-anomer at the reducing end of the xylobioside. The distorted peak near 4.8 ppm is due to the residual signal of water.

covalently modified peptide containing Glu78 (m/z of 826 in neutral loss mode) as observed in a previous analysis of WT BCX (Miao *et al.*, 1994; and data not shown). Finally, the crystal structure of the N35D BCX glycosyl-enzyme intermediate (N35D-2FXb) clearly shows covalent modification at Glu78 by the DNP2FXb inhibitor (details discussed subsequently).

Third, the role of Glu172 was also probed by site-directed mutagenesis. Analysis of the activity of the double mutant protein N35D/E172Q indicated that Glu172 still plays a primary role in functioning as the general acid/base catalyst in N35D BCX. This is not surprising, given the structural similarity of the mutant and WT enzymes (Figure 2), and thus the conserved positioning of the side-chain of Glu172 with respect to the binding site for xylosic substrates. Specifically, similar values of k_{cat}/K_m for hydrolysis of $ONPX_2$ were found for both the N35D/E172Q double mutant protein (0.021 s^{-1} mM^{-1}) and the E172Q single mutant protein (0.075 s^{-1} mM^{-1}) (Table 5). Note that this synthetic substrate has an activated leaving group that needs less general acid catalytic assistance for departure. Therefore, activity is observed, albeit at a substantially reduced rate, even with BCX variants lacking their general acid catalyst.

Brønsted analysis of the activity of N35D BCX towards aryl β-xylobiosides

The enzymatic activity of N35D BCX was measured using a number of different synthetic aryl β-xylobiosides of varying leaving group ability (Table 5). $ONPX_2$ was chosen as a reference substrate to compare the activities of all the BCX variants considered in this study. As summarized in

Table 5, at pH 6, N35D BCX has similar hydrolytic activity toward $ONPX_2$ ($k_{cat}/K_m = 0.56\ s^{-1}\ mM^{-1}$) compared to the WT enzyme ($k_{cat}/K_m = 0.66\ s^{-1}\ mM^{-1}$). Note, however, that the activity of N35D BCX is underestimated in this case, because measurements of k_{cat} and K_m were performed above its pH optimum of 4.6 and closer to the pH optimum of the WT protein.

Brønsted plots illustrating the dependence of log k_{cat} and log k_{cat}/K_m *versus* pK_a of the leaving group showed a similar dependence of rate on the pK_a of the departing phenol moiety for both WT ($\beta_{1g} = -0.5$, correlation coefficient = 0.88 (Lawson *et al.*, 1997)) and N35D BCX ($\beta_{1g} = -0.4$, correlation coefficient = 0.88) (plots not shown). The data unfortunately exhibit substantial scatter, perhaps due to the placement of the nitro substituent, which may differentially influence the binding of the substrate in the two cases and obscure the electronic effects of interest. However, the trend is clear and the general dependence of k_{cat} on the leaving group pK_a indicates that the glycosylation step is rate-limiting in the hydrolysis of aryl β-xylobiosides, since only the glycosylation step is influenced by the nature of the leaving group. Also, within the limits to which we can trust these Brønsted coefficients, there is a similar extent of negative charge development on the departing phenolate oxygen atom for the two proteins. Pre-steady-state kinetic studies of N35D BCX further confirmed that glycosylation is the rate-limiting step, since no observable burst phase was detected under a variety of conditions (data not shown). That is, no enzyme intermediate accumulated, since the initial glycosylation step was slower than the subsequent deglycosylation step. Together, these data reveal that the rate-limiting step for hydrolysis of aryl xyloside substrates has not changed as a result of a substitution of Asp for Asn35.

Studies of the N35D BCX glycosyl-enzyme intermediate

Use of the mechanism-based inhibitor or ''slow substrate'' DNP2FXb has allowed for trapping and subsequent analysis of the WT BCX glycosyl-enzyme intermediate (WT-2FXb) by ESMS, X-ray crystallography and NMR spectroscopy (McIntosh *et al.*, 1996; Miao *et al.*, 1994; Sidhu *et al.*, 1999). N35D BCX is also readily inhibited in a time-dependent manner by DNP2FXb (Figure 5). The kinetics of inhibition followed a pseudo-first-order scheme with values of the inhibition rate constant, $k_i = 0.68\ min^{-1}$, and of the inhibitor dissociation constant, $K_i = 10.5$ mM, at pH 4.1 and 40 °C. Since the DNP2FXb inhibitor has limited solubility under the conditions employed, values of k_i and K_i are only estimates. However, as has been noted, the value of the second-order rate constant for the reaction of inhibitor and enzyme, k_i/K_i, is reasonably accurate (Miao *et al.*, 1994). The value of k_i/K_i for N35D was determined from the slope of the reciprocal plot and found to be $0.065\ min^{-1}\ mM^{-1}$.

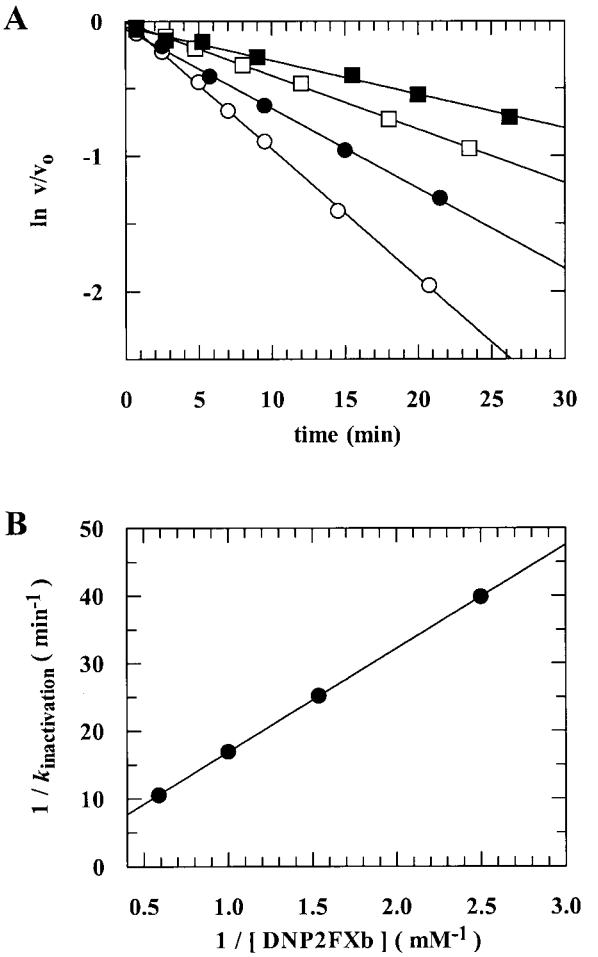

Figure 5. Time-dependent inhibition of N35D BCX by DNP2FXb at pH 4.1 and 40 °C. (a) Semi-logarithmic plot of residual activity (v/v_0) *versus* time at various concentrations of DNP2FXb: (■) 0.40 mM; (□) 0.65 mM; (●) 1.00 mM; and (○) 1.70 mM. (b) Inverse plot of the pseudo-first-order rates measured in (a) *versus* inhibitor concentration yielded a value of $0.065\ min^{-1}\ mM^{-1}$ for the second-order rate constant, k_i/K_I, determined from the slope of the plot.

This is reduced by only fivefold compared to the value obtained for the WT protein ($k_i/K_i = 0.34\ min^{-1}\ mM^{-1}$, $k_i = 2.2\ min^{-1}$, $K_i = 6.4$ mM at pH 6.0 and 40 °C) (Miao *et al.*, 1994).

Structure of the N35D BCX glycosyl-enzyme intermediate

The structure of the N35D BCX glycosyl-enzyme intermediate (N35D-2FXb) was determined at pH 7.5 to a resolution of 1.8 Å with an *R*-factor of 19.3 % (Tables 1 and 2). As seen with WT BCX, no significant change occurs in the backbone structure of N35D BCX upon formation of the covalent intermediate, except for a small displacement of the loop region (residues 111-125) over the active-site cleft (Connelly *et al.*, 2000; Sidhu *et al.*, 1999). The

most pronounced change is the covalent attachment of a 2-fluoro-xylobiosyl (2FXb) moiety to the $O^{\varepsilon 2}$ atom of Glu78 *via* an α-anomeric linkage with the C-1 atom of the proximal saccharide (Figure 6). The presence of this covalent attachment confirms that Glu78 functions as the nucleophile in N35D BCX and that hydrolysis proceeds through a double-displacement mechanism. In addition, the side-chain carboxyl group of Glu172 remains positioned to serve as a general acid and donate a proton to the oxygen atom of the aglycone leaving group during formation of the glycosyl-enzyme intermediate and, in turn, as a general base to facilitate deglycosylation by a nucleophilic water molecule. This provides strong support for the role of Glu172, at least in part (see Discussion), as a general acid/base catalyst in both the WT and mutant enzymes. Furthermore, the interactions between the protein side-chains and the 2FXb moiety in the N35D intermediate are also almost identical with those occurring in the WT intermediate, as discussed extensively by Sidhu *et al.*, (1999). Most notably, the distal xylose residue is stacked against Trp9 and forms hydrogen bonds to Tyr166 and Tyr69, whereas the proximal distorted xylose residue extensively hydrogen bonds to Tyr69, Arg112 and Pro116. Finally, the proximal saccharide is distorted to a $^{2,5}B$ (boat) conformation, whereas the distal saccharide is maintained in the conventional $^{4}C_1$ (chair) conformation in the glycosyl-enzyme intermediate of both WT (Sidhu *et al.*, 1999) and N35D BCX.

A comparison of the structures of the covalent intermediates of WT and N35D BCX reveals only two notable differences. Firstly, the distance between Glu172 $O^{\varepsilon 1}$ and a water molecule, that has been proposed to function as the nucleophile in the deglycosylation step (Sidhu *et al.*, 1999), is increased by ~0.7 Å in the N35D complex compared to the WT complex (Table 3). Second, and most significantly, the distance between Asn35 $N^{\delta 2}$/Asp35 $O^{\delta 2}$ and Glu172 decreases from 3.3 Å in WT-2FXb to 2.7 Å in N35D-2FXb. A small rotation of ~15° (χ_3) also increases the co-planarity of the two carboxyl groups. This is suggestive of a strong hydrogen bonding interaction between the side-chains of Asp35 and Glu172 in the N35D BCX glycosyl-enzyme intermediate at pH 7.5.

pK_a measurements of the N35D BCX glycosyl-enzyme intermediate

The pK_a of Glu172 in N35D BCX inhibited with DNP2FXb was directly measured by NMR spectroscopy (Figure 7). The ^{13}C-NMR spectra of N35D-2FXb BCX are very similar to those of WT-2FXb BCX (McIntosh *et al.*, 1996), allowing the carbonyl resonances to be readily assigned. Comparison to the data in Figure 3 reveals that N35D-2FXb and unmodified N35D BCX are markedly different in both chemical shift and titration behavior. Upon formation of the glycosyl-enzyme intermediate in N35D BCX, the δ-^{13}C resonance of Glu172 moves downfield by 1.4 ppm to 180.41 ppm, while the resonance of Glu78 moves upfield by almost 6.4 ppm to 175.94 ppm at neutral pH. The carbonyl resonance of Glu78 is essentially invariant with pH and shows no deuterium isotope shift (data not shown), as would be expected due to its covalent attachment to the 2-deoxy-2-fluoro-β-xylobiose. A minor shift with an apparent pK_a of 9.3 ($\Delta\delta = 0.18$ ppm) is observed for Glu78, which probably

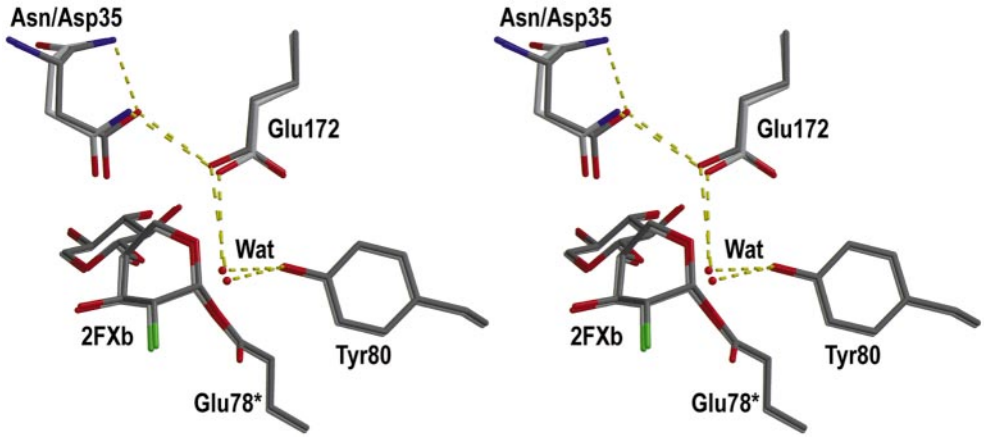

Figure 6. A stereo-illustration of the structural conformations of key active-site residues of the N35D BCX glycosyl-enzyme intermediate (N35D-2FXb) (dark gray) superimposed upon those of the WT glycosyl-enzyme intermediate (WT-2FXb) (light gray) (pH 7.5). Potential hydrogen bonds are indicated by broken yellow lines, oxygen atoms are shown in red and nitrogen atoms in blue. Modified Glu78-2FXb (Glu78*) is covalently attached to a 2-fluoroxylobiosyl (2FXb) moeity where the proximal saccharide is distorted to a $^{2,5}B$ conformation in both N35D-2FXb and WT-2FXb. A crystallographically identifiable water (Wat) molecule that is proposed to function in the deglycosylation step of the reaction is indicated by a red sphere. The most notable change is a reduction in the distance between Asn35 $N^{\delta 2}$/Asp35 $O^{\delta 2}$ and Glu172 from 3.3 Å in WT-2FXb to 2.7 Å in N35D-2FXb. See Table 3 for a listing of additional interatomic distances.

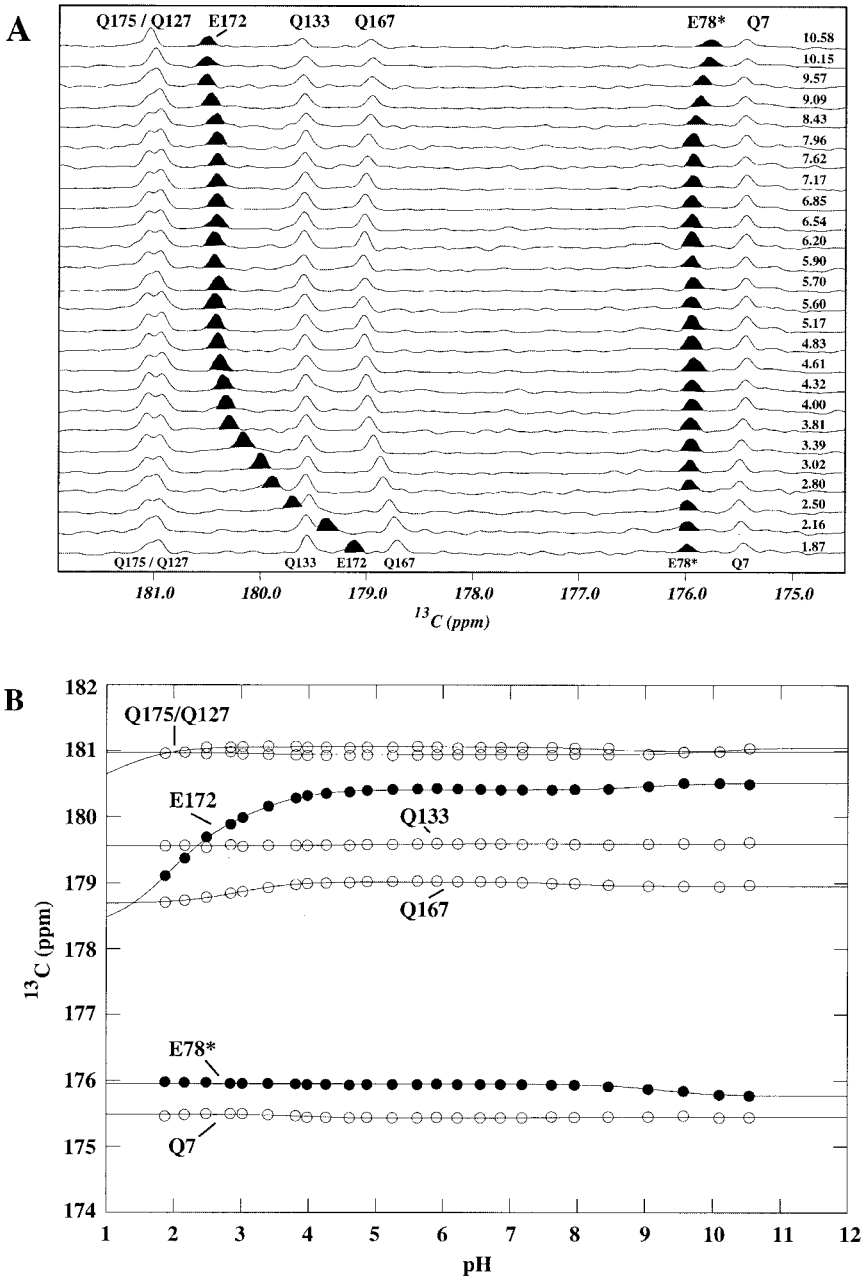

Figure 7. (a) pH-dependence of the ^{13}C-NMR spectra of N35D BCX covalently inhibited at Glu78 with 2FXb (25 °C). Resonance assignments were based on previously collected data for inhibited WT BCX (McIntosh *et al.*, 1996) and the spectra displayed as in Figure 2(a). The resonance of modified Glu78-2FXb (E78*) was distinguished from that of Gln7 by a lack of a hydrogen-deuterium isotope shift (not shown). The peaks corresponding to Glu172 and modified Glu78-2FXb are highlighted in black for emphasis. (b) Apparent pK_a values were determined for the two Glu residues (●) (Table 4) and the five Gln residues (○) by fitting to equations describing one or more sequential ionization equilibria.

reflects a pH-dependent change occurring at another site on the protein (Table 4). In contrast to the situation with unmodified N35D BCX, Gln7 and Gln127 no longer show pH-dependent shifts, thus confirming the dependence of their resonance frequencies on the charge state of Glu78.

After covalent modification of Glu78, Glu172 is the only titratable glutamic acid residue in N35D-2FXb BCX and thus its ^{13}C-NMR resonance is readily identifiable in the spectra shown in Figure 7. However, the pK_a of this residue is difficult to estimate from these data, since no titration baseline is observed in the acidic range, and thus a lower chemical shift limit could not be established. Nevertheless, fitting the data to a model involving three ionizations yielded very approximate apparent pK_a values of 1.9 ($\Delta\delta = 1.63$ ppm), 3.4 ($\Delta\delta = 0.48$ ppm) and 9.0 ($\Delta\delta = 0.10$ ppm). A single

pK_a of ~2.6 is obtained when the data are analyzed assuming one ionization event in the acidic range, although the fitting is less satisfactory.

To further investigate the ionization behavior of Glu172 in the glycosyl-enzyme intermediate of N35D BCX, deuterium isotope shift measurements were carried out. Comparison of the spectra of the covalently modified protein in 10% ^2H_2O and 90% ^2H_2O buffer at pH* 5.90 unambiguously shows that the carbonyl group of Glu172 has an isotope shift of −0.16 ppm. This value is midway between that of 0 ppm measured for deprotonated Glu78 in the uninhibited form of N35D BCX and −0.29 ppm for protonated Glu172. Possible interpretations of this result are that, in the glycosyl-enzyme intermediate, Glu172 is either ~50% protonated at pH 5.9 or is fully protonated yet with significantly reduced O-H covalent bond character. This observation poses an interesting problem, given that Glu172 should be fully deprotonated at pH 5.9 if its pK_a value is indeed less than 3.4, as suggested by the titration data of Figure 7. One plausible explanation of this behavior is that, upon formation of the glycosyl-enzyme intermediate, the microscopic pK_a of Glu172 drops to a value in the range of 1.9 to 3.4 such that it is approximately equal to that of Asp35. Although we did not measure the pK_a of residue 35 in this system, due to the large number of aspartic acid and asparagine residues in N35D-2FXb BCX (and thus the need to reassign the δ-carbonyl resonances in the modified protein), it is reasonable to assume that its pK_a would not increase significantly from the value of 3.7 found in the uninhibited form of N35D BCX. Given that these two residues have intimately associated carboxyl groups, as shown crystallographically (Figure 6), as well as comparable pK_a values, they may in effect behave as a single, coupled unit. The first proton of the pair can be lost in the titration event corresponding to the apparent pK_a value of 1.9 or 3.4 measured from the pH-dependent chemical shift of Glu172, or to a single pK_a of 2.6 obtained when the data are fitted to one ionization event in the acidic range. (This argument recognizes the difficulty of differentiating the effects of the ionization of Glu172 or Asp35 on the chemical shift of the carbonyl group of Glu172, and thus the ambiguity in the interpretation of the fitted pK_a values.) Consistent with the observed separation of only 2.7 Å between O^δ of Asp35 and O^ε of Glu172 (Figure 6), this leaves a single proton shared in an ionic hydrogen bond between two residues at neutral pH values. Thus the deuterium isotope effect of −0.16 ppm would be attributed to the effects of strong hydrogen bonding, rather than partial protonation *per se*. This is reminiscent of the description of a so-called low barrier hydrogen bond (LBHB). However, we did not observe the signal from an unusually downfield-shifted proton in the ^{1}H-NMR spectrum of N35D-2FXb BCX at pH* 6.1 and 25 °C that is often attributed to a proton in an LBHB.

To complete this argument, we must define the pK_a for the loss of the second proton from the Asp35-Glu172 pair of N35D-2FXb BCX. From the titration data shown in Figure 7, the carbonyl chemical shift of Glu172 remains approximately constant in the alkaline range up to a pH of 10.6. Only a small change of 0.1 ppm, fitting an apparent pK_a of 9.0, was observed. Although not impossible, it seems unlikely that this small shift reflects the deprotonation of Glu172, suggesting that the actual pK_a value for the loss of the second proton must be >11. However, based on this uncertainty, we conservatively conclude that the pK_a for the second ionization of Asp35-Glu172 is >9. This represents a perturbation of at least 5.5 units from the value of the first ionization, or an energetic interaction of >9 kcal mol^{-1} disfavoring the juxtaposition of Asp35 and Glu172 in their negatively charged forms.

The low pK_a of the Asp35-Glu172 pair in the glycosyl-enzyme intermediate of N35D is consistent with the phenomenon of pK_a cycling that occurs in retaining glycosidases (McIntosh *et al*., 1996). In a retaining glycosidase, the pK_a of the general acid/base cycles to match its catalytic role as a general acid in the glycosylation step (higher pK_a) or a general base in the deglycosylation step (lower pK_a). Previous studies of BCX using DNP2FXb to trap the glycosyl-enzyme intermediate have shown that the pK_a of Glu172 cycles from 6.7 in the free WT enzyme when it functions as a general acid to 4.2 in the enzyme intermediate when it functions as a general base (McIntosh *et al*., 1996). Hence, a lower pK_a measured for the Asp35-Glu172 pair in the glycosyl-enzyme intermediate of N35D BCX indicates that this carboxyl pair can play a dual catalytic role as a general acid and as a general base in the double-displacement hydrolysis reaction.

Discussion

Overview

Substitution of an aspartic acid for an asparagine residue at position 35 results in a pronounced change in the pH optimum of BCX from pH 5.7 to 4.6 and a slight increase in activity. The acidic and basic limbs of the activity profile follow apparent pK_a values of 3.5 and 5.8, respectively. The net effect of this substitution is to change BCX from an ''alkaline'' towards an ''acidic'' xylanase. X-ray crystallographic structural studies showed that the structure of N35D BCX closely resembles that of WT BCX, with the exception of a small increase in distance between the carboxyl groups of Asp35 and Glu172 (3.1 Å in WT and 3.2 Å in N35D). Consistent with the lack of any structural perturbation, N35D BCX still follows a retaining mechanism, in which glycosylation is rate-limiting. In addition, the kinetics of inhibition of N35D and WT BCX with DNP2FXb are similar.

To explain the observed shift in pH optimum, we used ^{13}C-NMR to directly measure the pK_a

values of the catalytically essential residues in both the free enzyme and in the glycosyl-enzyme intermediate of N35D BCX. In the free enzyme, the apparent pK_a of the newly introduced Asp residue at position 35 is 3.7, while those of Glu78 and Glu172 are elevated from their WT values to 5.7 and 8.4, respectively. The ionization states at pH 6.3 expected from the pK_a values of Asp35, Glu78 and Glu172 were confirmed by deuterium isotope shift measurements. Thus, the activity profile of N35D BCX appears to follow the pK_a values of Asp35 and Glu78, instead of Glu78 and Glu172 as in WT BCX. However, several experiments confirmed that Glu78 is still the nucleophile and that Glu172 still contributes to the role of the general acid catalyst.

The crystal structure of the N35D BCX glycosyl-enzyme intermediate is very similar to that of the WT glycosyl-enzyme intermediate, with a significantly notable exception. The side-chain carboxyl groups of Asp35 and Glu172 are now shifted closer together (2.7 Å in N35D-2FX *versus* 3.3 Å in WT-2FXb) with a concomitant increase in co-planarity. The energetic driving force for the favorable juxtaposition of these two carboxylate groups apparently arises from the formation of a rather short and strong hydrogen bond resulting from the loss of the first proton and the subsequent sharing of the second between these two groups. This conclusion is supported by ^{13}C-NMR titrations, which indicate that Glu172 and Asp35 behave as a single coupled unit with a pK_a in the range of 1.9 and 3.4 for the loss of the first proton and a pK_a of >9 for the loss of the second, combined with the observation of an intermediate deuterium isotope shift at pH 5.9, indicative of a shared proton bridging these two carboxylate groups.

pK_a values of the catalytic residues

Previous NMR studies of WT BCX revealed that Glu78 and Glu172 have coupled ionization equilibria. Consistent with their catalytic roles, the major pK_a values for these two residues are 4.6 and 6.7, respectively. However, when their biphasic titration curves were fitted to a model describing the interaction of two ionizable groups, the microscopic pK_a of Glu172 in the presence of a neutral Glu78 was found to be 5.5, and that of Glu78 in the presence of a charged Glu172 was 5.8 (see Scheme 1 of McIntosh *et al.*, 1996). Therefore, the electrostatic interaction between the two nearby carboxyl groups (C^{δ} separation = 6.5 Å) perturbs their pK_a values by ~1.2 units. This is supported by the observation that upon substitution of Glu78 with Gln, the pK_a of Glu172 drops to 4.2, whereas the reciprocal mutation of Glu172 leads to a slight elevation of the pK_a of Glu78 to 5.0. In both cases, the titration curves become monophasic. The differences between the pK_a values measured for the mutant proteins and those determined from an analysis of the biphasic titration curves of WT BCX suggest that the coupling between the two glutamic acids is not purely electrostatic. Conformational changes in the active-site upon ionization or mutation may also influence the titration behavior of Glu78 and Glu172.

Substitution of Asn35 to an aspartic acid residue leads to a dramatic change in the ionization properties of BCX. Most notably, the apparent pK_a values of Glu78 and Glu172 are elevated to 5.7 and 8.4, respectively, and both residues show triphasic titration curves. This undoubtedly arises from an additional electrostatic interaction with Asp35, which has an apparent pK_a of 3.7 and thus is predominantly in a negatively charged state at pH values when Glu78 and Glu172 undergo deprotonation. The greater perturbation of the pK_a value of Glu172 is consistent with the crystal structure of N35D BCX, determined at pH 7.5. That is, the carboxyl carbon atoms of Asp35 and Glu172 are separated by 4.8 Å, whereas those of Asp35 and Glu78 are 8.5 Å apart (Figure 2 and Table 3).

The multiphasic titration curves recorded for Asp35, Glu78, and Glu172 clearly indicate a complex network of electrostatic, and possibly structural, interactions between these three residues. As outlined in Results, the apparent pK_a values listed in Table 4 were determined by fitting the NMR-detected titration curves of the active-site carboxyl groups to a simple model of sequential ionization events. However, to gain further insight into the electrostatic interactions between Asp35, Glu78, and Glu172, it is useful to analyze their titration data to extract microscopic pK_a values. Unfortunately, with eight possible ionization states, it is difficult to carry out this analysis in full. Using only data recorded in acidic solutions (e.g. with Glu172 protonated), a simultaneous fitting of the titration curves for Asp35 and Glu78 to a model of two coupled ionization equilibria yields the microscopic pK_a values shown in Scheme 1:

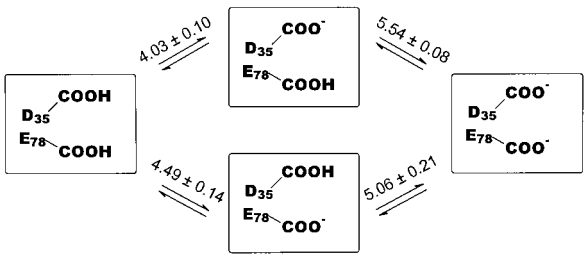

Scheme 1.

The upper limb of this scheme shows the predominant ionization pathway of N35D BCX in which Asp35 deprotonates with increasing pH before Glu78, whereas the lower corresponds to the minor population of protein in which Glu78 is negatively charged and Asp35 neutral. Note that the microscopic pK_a of 5.54 for Glu78 along the upper limb of this coupled equilibrium curve is similar to the apparent pK_a value of 5.7 listed in Table 4, whereas that of 4.03 for Asp35 is somewhat higher than the

corresponding value of 3.7 determined from a sequential ionization model. This reflects the difficulty of extracting pK_a values for complex binding equilibria in proteins, as the chemical shifts of involved residues are exquisitely sensitive to both structural and electrostatic factors, thus the equations describing their NMR behavior are underdetermined experimentally. However, support for Scheme 1 follows from the observation that the microscopic pK_a of 4.49 fit for Glu78 in the presence of a neutral Asp35 is very similar to that of 4.6 measured for this catalytic residue in WT BCX, which contains a neutral asparagine residue at position 35. Recognizing that the accuracy of these fittings is uncertain, Scheme 1 suggests that the ionization of Asp35 elevates the pK_a of Glu78 by ~1 unit, and *vice versa*, due to charge repulsion, with an energetic coupling of $2.303RT(\Delta pK_a) \cong 1.4$ kcal mol^{-1}. The implications of this analysis for understanding the catalytic mechanism of N35D BCX will be discussed below.

Unfortunately, we were unable to extract microscopic pK_a values for the coupling of Glu172 with Glu78 or Asp35 for the following two reasons. First, in contrast to the case of the WT protein, upon addition of acid, the $^{13}C^{\delta}$ nuclei of Glu78 and Glu172 in N35D BCX show small downfield shifts (i.e. opposite to that expected for protonation of a carboxylate) at pH values corresponding to each other's pK_a values. Therefore, it is not possible to fit these data to the equation describing the pH-dependence of the chemical shifts of two residues with coupled ionization equilibria (Shrager *et al.*, 1972). Second, NMR data were not recorded above pH 8.3 for [γ-^{13}C]Asp-labelled N35D BCX, thus precluding a mutual fit of the titration curves of Asp35 and Glu172 for microscopic pK_a values. However, due to the large difference in their apparent pK_a values, the population of protein with Asp35 protonated and Glu172 deprotonated must be negligible.

Upon formation of a long-lived glycosyl-enzyme intermediate, the pK_a value of Glu172 in WT-2FXb BCX drops from 6.7 to 4.2 (McIntosh *et al.*, 1996). This pK_a cycling allows the glutamate residue to perform its dual role as a general acid for the glycosylation step and general base for deglycosylation. The reduction in the pK_a value of Glu172 by 2.5 units is attributed to the elimination of charge repulsion from Glu78, due to formation of a covalent linkage to the 2-fluoro-xylobiose, as well as to possible changes in the structure and hydration of BCX (McIntosh *et al.*, 1996). In a similar fashion, formation of the N35D BCX glycosyl-enzyme intermediate leads to a dramatic change in the titration behavior of Glu172. As seen in Figure 7, the pH-dependence of the δ-^{13}C resonance of Glu172 follows apparent pK_a values of 1.9 or 3.4 when fitted to two sequential titrations or 2.6 when fitted to one ionization event in the acidic range. The observation of an isotope shift of -0.16 ppm at pH* 5.90 for Glu172 indicates that this residue is at least partially protonated at pH values above these pK_a values.

Based on this measured titration and deuterium isotope shift data, we conclude that Asp35 and Glu172 are behaving as a highly coupled dicarboxylic acid system in N35D-2FXb BCX, with a first pK_a in the range of 1.9-3.4 and a second estimated to be >9. This is remarkable for two reasons. First, in the case of the WT enzyme, the pK_a of Glu172 drops by only 2.5 units upon covalent modification of Glu78, whereas in N35D BCX, the pK_a value associated with Glu172 falls by ~5.8 units, from 8.4 to ~2.6. Second, assuming that the pK_a values for the first and second deprotonation steps of the Asp35-Glu172 pair are ~2.6 and >9, this represents an energetic interaction of >9 kcal mol^{-1} disfavoring the juxtaposition of the two carboxylate groups in their negatively charged forms. A possible explanation for this behavior is seen from a comparison of the crystal structures of N35D BCX in its free and modified forms, determined at pH 7.5. In the free enzyme, the distance between Asp35 $O^{\delta 2}$ and Glu172 $O^{\varepsilon 2}$ is 3.2 Å, whereas in the glycosyl-enzyme intermediate, the separation is reduced to 2.7 Å (Table 3). The corresponding values for the WT protein are 3.1 Å and 3.3 Å, respectively. This suggests that a relatively strong hydrogen bond exists between Asp35 and Glu172 in N35D-2FXb BCX, such that one proton is shared between the two carboxyl groups with a net charge of -1. As mentioned previously, this interaction shares many similarities to an LBHB, in that a proton is partitioned somewhat equally between the two carboxylate groups with first ionization pK_a values that are approximately matched. However, the signature proton with a downfield-shifted resonance commonly attributed to the presence of an LBHB is not detected. Also, although slightly less than the ~2.8 Å oxygen-oxygen hydrogen bonding distance observed in water, the Asp35-Glu172 separation is somewhat longer than the value of <2.55 Å often cited for such an LBHB in model compounds (Cleland *et al.*, 1998). Regardless, this close interaction between these two active-site residues, which is not observed in WT-2FXb BCX, could account for the distinct pK_a values measured for Glu172 in the mutant enzyme. By way of comparison, in a study of the ionization of symmetric dicarboxylic acids, McDaniel & Brown (1953) reported that the pK_a values for *cis*-caronic acid were 2.3 and 8.2. This strong energetic coupling was attributed to a highly favorable hydrogen bond between a carboxylic acid and a carboxylate group in this constrained ring system.

Reverse protonation mechanism

Based upon the pK_a values of Glu78 (5.7) and Glu172 (8.4) determined by ^{13}C-NMR, and by analogy to the WT enzyme, the pH optimum of N35D

BCX is expected to be ~7.0. However, in marked contrast, the observed pH-dependence of k_{cat}/K_m, which reflects ionizations in the free enzyme, yields a pH optimum of 4.6 and a bell-shaped activity profile with apparent pK_a values of 3.5 and 5.8. Therefore, it appears that the pH-dependent activity of N35D BCX is determined by the ionization states of Asp35 and Glu78, rather than Glu172 and Glu78 as seen with the WT protein. However, since Glu78 must still be deprotonated to serve as a nucleophile, it follows that Asp35 must be protonated in the active enzyme. This situation, in which enzymatic hydrolysis requires that the group with the higher pK_a be deprotonated while that with the lower pK_a remains protonated, has been termed ''reverse protonation'' (Mock & Aksamawati, 1994). Although somewhat unintuitive, this reversed ionization scheme will also give rise to a bell-shaped activity profile with apparent pK_a values for the acidic and basic limbs closely matching those of the two ionizable groups (Figure 8). However, in contrast to the more frequently observed cases exemplified by WT BCX, only a small percentage of the enzyme is in the correct ionization state for catalysis to occur. This kinetic mechanism has been invoked to explain the pH-dependence of the activities of several enzymes, including thermolysin, urease, and aspartate transcarbamylase (Karplus *et al*., 1997; Mock & Aksamawati, 1994; Mock & Stanford, 1996; Turnbull *et al*., 1992).

Upon closer examination, several fundamental questions arise in attempting to explain the activity of N35D BCX, as well as other acidic xylanases, in terms of a reverse protonation mechanism. First, as is clearly shown in Figure 8, on the basis of their spectroscopically measured apparent pK_a values, the fraction of the enzyme with Asp35 and Glu78 in the correct ionization states is only ~1 %. Since the overall activity of N35D BCX is ~20 % greater than WT BCX at their respective pH optima, the mutant enzyme in a state with Asp35 neutral and Glu78 deprotonated must have an inherent catalytic efficiency at least two orders of magnitude higher than that of the parental WT. Why, then, is this enzyme species such an efficient catalyst? Second, this mechanism implies that N35D BCX is inactive when Asp35 is deprotonated, even though Glu172 (p$K_a = 8.4$) still bears a proton. Furthermore, Glu172 is positioned structurally to donate a proton to the aglycone oxygen atom during the glycosylation reaction and to abstract a proton from a water molecule during the subsequent deglycosylation reaction (Figures 2 and 6). Why can Glu172 not act alone as the general acid/base catalyst under these conditions to allow hydrolysis at elevated pH values?

A possible answer to these two questions lies with the observation of a short hydrogen bond between Asp35 and Glu172 in the glycosyl-enzyme intermediate. A series of elegant model studies carried out by Kirby using small-molecule systems to probe intramolecular proton transfer in the acid-catalyzed hydrolysis of acetals revealed that extremely effective intramolecular acid catalysis occurs when a strong hydrogen bond is formed between

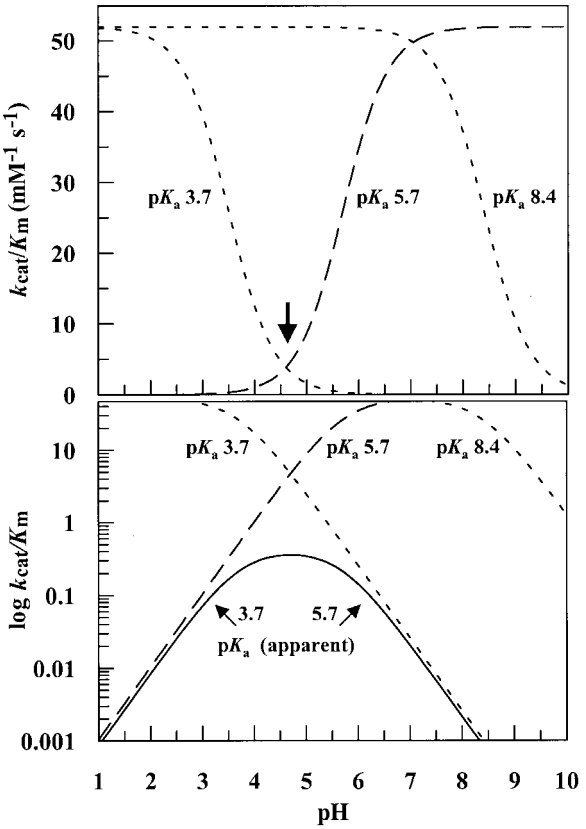

Figure 8. Simulated activity profiles for the proposed reverse protonation mechanism of N35D BCX. In the upper panel, titration curves are generated for the deprotonation of Glu78 (pK_a 5.7, – – –) and the protonation of Asp35 (pK_a 3.7, -----) and Glu172 (pK_a 8.4, -----). If N35D BCX behaved like the WT enzyme, optimal activity would be observed at pH ~7, where Glu78 is deprotonated and Glu172 protonated. In contrast, to explain the observed pH optimum of 4.6, we propose that Asp35 is protonated in the active form of the enzyme to function as the general acid along with Glu172, while Glu78 is depronated to serve as a nucleophile. Since the pK_a of Glu78, measured by NMR spectroscopy, is greater than that of Asp35, the required combination of ionization states occurs only in the small region of overlap between the titration curves of these two residues (arrow). This is illustrated in the lower panel, where the product of the two titration curves is shown as a continuous line and the scale of k_{cat}/K_m is logarithmic. Fitting to the standard equation for a bell-shaped activity profile yields apparent pK_a values of 3.7 and 5.7. This verifies that both normal and reverse protonation mechanisms yield bell-shaped activity curves with apparent pK_a values matching those measured for the two groups whose ionization states dictate the activity of the enzyme. Note, however, with the latter mechanism, N35D BCX has only ~1 % of the activity that it would have in a theoretical state with Asp35 fully protonated and Glu78 fully deprotonated. The curves in this Figure were scaled to match the observed maximum value k_{cat}/K_m of 0.43 s^{-1} mM^{-1} measured with $ONPX_2$ at 25 °C (Figure 1).

the departing alcohol and the conjugate base form of the general acid catalyst in systems such as that shown in Scheme 2 (Kirby, 1997). This strong hydrogen bond must exist, at least in part, in the transition state leading to the product, thereby stabilizing it and facilitating hydrolysis.

The situation observed with N35D BCX is

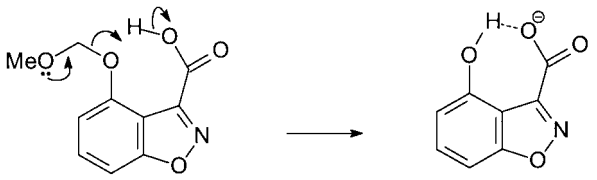

Scheme 2.

directly analogous to these model systems, since a strong hydrogen bond is formed between Asp35 and Glu172 in the glycosyl-enzyme intermediate. This hydrogen bond is stronger (shorter) than that in the free enzyme, largely as a consequence of the removal of charge from Glu78 upon formation of the glycosyl-enzyme intermediate. Stated equivalently, elimination of repulsive Coulombic interactions, by formation of an ester on Glu78, lowers the pK_a value of Glu172 to more closely match that of Asp35, thereby allowing Asp35-Glu172 to function together as an efficient general acid. Even though this strong hydrogen bond is not formed between the acid/base catalyst and the departing aglycone oxygen atom, as in the cases studied by Kirby, the effect is the same, since the glycosyl-enzyme intermediate, and therefore the transition states leading to it, are stabilized (Figures 9 and 10). Indeed, this situation is preferable in a catalytic system since, were the hydrogen bond formed to the aglycone oxygen atom, product dissociation could be significantly slowed.

The question then arises as to whether the hydrogen bond formed is strong enough to lower the activation energy for glycosyl-enzyme intermediate formation sufficiently to account for the inherently 100-fold more efficient enzyme. An answer to this lies in the observation made previously (Richard, 1998), on the basis of our earlier demonstration of pK_a cycling in BCX (McIntosh *et al.*, 1996), that the chemical step of covalent glycosyl-enzyme intermediate formation is closely coupled to the ionization behavior of the key active-site carboxylic acids. Thus the observed shift in the pK_a value of the acid/base catalyst upon formation of the glycosyl-enzyme intermediate in effect drives its formation. The pK_a shift of 2.5 units in WT BCX corresponds to an energy difference of 3.5 kcal mol^{-1}. In the case of N35D BCX, the very large pK_a shift of 5.8 units from 8.4 to ~2.6 for Glu172, which represents an energy difference of ~8 kcal mol^{-1}, is indeed sufficient to overcome the fact that only a very small percentage of the enzyme is in the correct ionization state for catalysis. It is interesting to note that the first pK_a of the Asp35-Glu172 system drops from 3.7 in the free enzyme to ~2.6 in the glycosyl-enzyme intermediate due to the removal of the charge on Glu78. Thus, at each point along the reaction coordinate leading to this intermediate, proton donation becomes more effective. The other question concerns why the monoprotonated Asp35-Glu172 system could not act as an effective acid catalyst, despite the pK_a value of 8.4 measured for the glutamic acid in the free enzyme. The answer to this lies in the unfavorable coupling of ionization behavior to glycosyl-enzyme intermediate formation in this case. This arises from the fact that glycosyl-enzyme formation results in an increase in the pK_a of Glu172 from 8.4 in the free enzyme to >9 for the Asp35-Glu172 pair in the covalent intermediate. Consequently, at each point along the

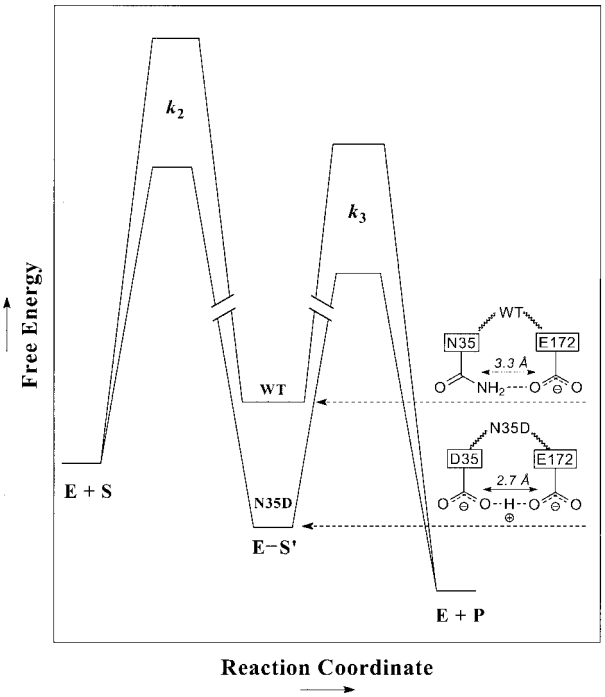

Figure 9. A schematic reaction-coordinate diagram illustrating how the formation of the highly favorable glycosyl-enzyme intermediate along the hydrolytic reaction pathway of N35D BCX increases its catalytic efficiency relative to WT BCX. The development of a short (2.7 Å) strong hydrogen bond between Asp35 and Glu172 leads to significant stabilization of the N35D BCX glycosyl-enzyme intermediate, and consequently, a reduction in the free energy barriers of the neighboring transition states for glycosylation (k_2) and deglycosylation (k_3) (lower trace). In contrast, the longer (3.3 Å) hydrogen bond formed between Asn35 and Glu172 in the glycosyl-enzyme intermediate of WT BCX does not lead to the same degree of stabilization and rate enhancement (upper trace). The energy levels of the free enzyme and substrate (E + S), the enzyme-intermediate (E-S′), and the free enzyme and product (E + P) are indicated qualitatively in this diagram.

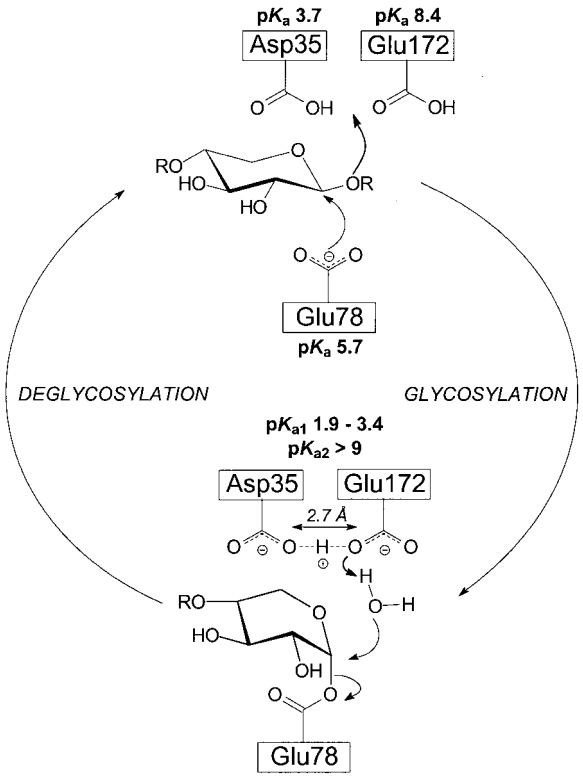

Figure 10. The proposed double-displacement retaining mechanism of N35D BCX. In the glycosylation step, Asp35 and Glu172 function together in serving the role of the acid/base catalyst, whereas deprotonated Glu78 is the nucleophile. In the glycosyl-enzyme intermediate, Asp35-Glu172 interact strongly with coupled ionizations, pK_{a1} 1.9-3.4 and $pK_{a2} > 9$. Due to this pK_a cycling, they can now serve as a general base in the deglycosylation step of the reaction.

reaction coordinate in this system, donation of the second proton from this carboxyl pair becomes less effective.

Although the two questions posed above regarding the catalytic efficiency of a reverse protonation mechanism can be resolved adequately, a rather subtle caveat to this mechanism should be noted. The current proposal of a reverse protonation mechanism follows from the similarities of the pK_a values determined from the activity profile of N35D BCX and the major ''apparent'' pK_a values of Asp35 and Glu78 measured by ^{13}C-NMR. However, if Asp35 is in a protonated state when the enzyme is catalytically active, we must in fact consider the microscopic pK_a values of Asp35 and Glu78, rather than their predominant or apparent pK_a values. According to this model, shown in Scheme 1, in the presence of a neutral Asp35, the pK_a of Glu78 is ~4.5 rather than ~5.5. Similarly, in the presence of a negatively charged Glu78, the pK_a of Asp35 is ~5 rather than ~4. This implies that the pH-dependent activity profile of N35D BCX should follow apparent pK_a values of ~4.5 (Glu78) and ~5 (Asp35). Since this is not observed, the analysis of the ^{13}C-NMR titration data according to Scheme 1 may not be appropriate for N35D BCX, due to the previously mentioned difficulties in interpreting the pH-dependent changes in the chemical shifts of carboxyl groups. However, irrespective of the details of the analysis, the pK_a values of Glu78 and Glu172 in the presence of a neutral Asp35 are expected to differ from those measured from the major pH-dependent change in their ^{13}C-NMR spectra due to electrostatic interactions between their closely juxtaposed side-chain carboxyl groups. Thus, the correspondence between the observed pK_a values of 3.5 and 5.8 from the pH-dependent activity profile of N35D BCX and 3.7 (Asp35) and 5.7 (Glu78) from NMR measurements is somewhat perplexing. Perhaps this expectation is false and the perturbation of the pK_a value of Glu78 due to the N35D substitution does not arise from electrostatic interactions, as implied in Scheme 1, but rather from very subtle structural differences between aspartic acid and asparagine side-chains. Thus in the presence of a neutral Asp35, Glu78 may still have a pK_a of ~5.7, and in the presence of a charged Glu78, Asp35 may still have a pK_a of ~3.7, corresponding to the limbs of the activity profile of N35D BCX. To address this issue, crystallographic studies of WT and N35D BCX at acidic pH values may be necessary.

In summary, a combination of NMR and kinetic studies demonstrates that the pH-dependent activity of N35D BCX, and by inference other ''acidic'' family 11 xylanases, is dictated by the ionization states of the nucleophile, Glu78, and the Asp35 residue adjacent to the general acid, Glu172. Although not without concerns, this can be explained by a reverse protonation mechanism in which Asp35 and Glu172 act together as the general acid and, subsequently, as the general base in the two-step hydolysis reaction (Figure 10).

Comparison to other xylanases

The correlation between the presence of an asparagine or an aspartic acid residue at position 35 (BCX numbering) and the ''alkaline'' or ''acidic'' pH optima of family 11 xylanases, repectively, is well recognized. As summarized below, three structural investigations aimed at understanding this phenomenon have been reported.

Torronen and Rouvinen examined two family 11 xylanases from *Trichoderma reesei* (Torronen & Rouvinen, 1995). XYNI is an acidic xylanase with an aspartic acid residue at position 33 and a pH optimum of 3.5, whereas XYNII is an alkaline xylanase with an asparagine residue at position 44 and a pH optimum of 5.3 (Table 6). In XYNI, Asp33 clearly makes a hydrogen bond (2.9 Å) to the acid/base catalyst (Glu164). In contrast, in XYNII, Asn44 is involved in a weaker interaction (3.4-3.7 Å) with the acid/base catalyst (Glu177). Without information regarding the pK_a values of the catalytic residues, or the ability to directly detect

Table 6. Properties of family G xylanases

Xylanase	pH optimum	pI[i]	Residue at position 35[j]	Distances (Å)[j] Asx35 $N^{\delta 2}/O^{\delta 2}$-Glu172 $O^{\varepsilon 2}$
B. agaradhaerens (Xyl11)[a]	11[a]	8.8	Asn	[k]
T. lanuginosus[b]	6.5[a]	4.7	Asn	3.0[l]
B. circulans (BCX)[c]	5.7[b]	9.1	Asn	3.1
T. reesei (XYNII)[d]	5.3[c]	8.7	Asn	3.6
B. circulans (N35D)[e]	4.6[d]	8.8	Asp	3.2
T. reesei (XYNI)[f]	3.5[e]	4.6	Asp	2.9
A. niger (xylanase I)[g]	3.0[f]	4.0	Asp	2.8
A. kawachii (XynC)[h]	2.0[g]	3.9	Asp	2.8

[a] *Bacillus agaradhaerens* xylanase (Xyl11) structure was solved at pH 5.0, PDB code 1QH7 (Sabini *et al*., 1999).
[b] *Thermomyces lanuginosus* xylanase structure was solved at pH 4.0, PDB code 1YNA (Gruber *et al*., 1998).
[c] *Bacillus circulans* xylanase (BCX) structure was solved at pH 7.5, PDB code 1XNB (Wakarchuk *et al*., 1994).
[d] *Trichoderma reesei* xylanase II (XYNII) structure was solved at pH 6.5, PDB code 1XYP (Torronen *et al*., 1994).
[e] *Bacillus circulans* xylanase variant N35D structure was solved at pH 7.5, PDB code 1C5H.
[f] *Trichoderma reesei* xylanase I (XYNI) structure was solved at pH 8.0, PDB code 1XYN (Torronen & Rouvinen, 1995).
[g] *Aspergillus niger* xylanase I structure was solved at pH 4.7, PDB code 1UKR (Krengel & Dijkstra, 1996).
[h] *Aspergillus kawachii* xylanase C (XynC) structure was solved at pH 6.5, PDB code 1BK1 (Fushinobu *et al*., 1998).
[i] Theoretical pI was calculated using the ''Compute pI/Mw tool'' resource located on the ExPASy server (Wilkins *et al*., 1998).
[j] Residue numbering and atom labelling is based on the sequence and structure of BCX.
[k] Coordinates not released from the RCSB Protein Data Bank at time of publication.
[l] Measured distances are based on a structure in which the acid/base catalyst, Glu178, is in an unfavorable conformation and points away from the nucleophile, Glu86 (Gruber *et al*., 1998).

their protonation states by X-ray diffraction, the authors suggested that, in XYNI, Asp33 is neutral and involved in a strong hydrogen bonding interaction that serves to lower the pK_a of Glu164 and thereby reduce the pH optimum of the enzyme. Based on our studies of N35D BCX, it seems likely that Glu164 in XYNI actually has a higher pK_a than Glu177 in XYNII, and that Asp33 is largely deprotonated under the experimental conditions used for this study.

In a crystallographic analysis of the acidic xylanase, *Aspergillus niger* xylanase I, Krengel and Dijkstra found that Asp37 and the acid/base catalyst (Glu170) were within close hydrogen bonding distance (2.8 Å) of each other, as had been observed for the analogous residues in *T. reesei* XYNI (Krengel & Dijkstra, 1996; Torronen & Rouvinen, 1995). Based on its solvent exposure, they proposed that Asp37 is negatively charged at the pH of crystallization (pH 8) and therefore serves to elevate the pK_a of Glu170. To explain the pH optimum of 3 measured for this enzyme, they suggested that xylanase I is active when Asp37 is protonated and inactive when it is deprotonated. At low pH when Asp37 is protonated, the proton of the general acid Glu170 is available for catalysis. However, at high pH, when Asp37 is deprotonated, the catalytic proton of Glu170 is suggested to be detained in an ionic hydrogen bond to this residue, thereby preventing hydrolysis at elevated pH values. Thus, according to this mechanism, the ionization state of Asp37 primarily dictates the acidic limb of the pH-dependent activity profile of this xylanase. Although no correlation of activity to the ionization state of the nucleophile (or measurement of its pK_a value) was given, this argument is essentially equivalent to the reverse protonation mechanism proposed herein to explain the activity of N35D BCX.

In a more recent study of the acidic xylanase from *Aspergillus kawachii*, xylanase C, Fushinobu *et al*. (1998) experimentally confirmed the essential role that an aspartic acid residue (Asp37) adjacent to the acid/base catalyst (Glu170) has in lowering the pH optimum of this family 11 xylanase. Xylanase C has a pH optimum of 2, one of the lowest of this family. Mutation of Asp37 to asparagine dramatically shifts the pH optimum of xylanase C from 2 to 5, albeit with an 85% reduction in xylanolytic activity. (This substitution is the reverse of that in N35D BCX.) In their structural analysis of the WT enzyme, they also observed the same short distance between Asp37 and Glu170 (2.8 Å) as was reported for the other acidic xylanases (Table 6).

A summary of the structural and enzymatic properties of these xylanases, plus those from *Bacillus agaradhaerens* and *Thermomyces lanuginosus*, is presented in Table 6. Although each of these enzymes shares a structurally similar arrangement of fully conserved active-site residues surrounding two catalytic glutamic acid residues, they exhibit pH optima spanning a remarkable range from approximately 2 to 11. While the presence of an aspartic acid or an asparagine residue at position 35 (BCX numbering) provides a clear division between those with ''acidic'' (<5) or ''alkaline'' (>5) optima, additional factors must also contribute to defining their pH-dependent activity profiles. One trend, evident from Table 6, is that, for the acidic enzymes, the shorter the distance between the acid/base catalyst and the adjacent aspartic acid residue, the lower the pH optimum of the xylanase. It is plausible that this reflects increasingly stronger hydrogen bonding between these residues, which would correlate with a reduction in

the pK_a of the Asp and hence a shift in the acidic limb of the activity profile of these enzymes to lower pH values. It would be particularly interesting to extend this analysis to the measurement of the same distances in the glycosyl-enzyme intermediates of these xylanases to see if the stabilization of the ''Asp-Glu'' general base is also correspondingly greater.

A second, albeit imperfect, trend seen in Table 6 is that naturally occuring acidic xylanases have low pI values, whereas alkaline xylanases tend to have high pI values. This is also somewhat counter-intuitive as, for example, a low pI indicates an excess of glutamic acid and aspartic acid residues, which by charge repulsion should disfavor low pK_a values for the active-site catalytic groups. However, with further inspection, we see that xylanases with pH optima below ~6 have theoretical pI values such that they should actually carry a net positive charge at their respective pH optima (e.g. pI >pH optimum). This may help lower the pK_a values of the catalytic carboxylic acid side-chains, and thereby allow activity under acidic conditions. In contrast, the two xylanases with pH optima above ~6 have pI values less than their pH optima, indicating that they will carry a net negative charge when maximally active. This may serve to elevate the pK_a values of the catalytic glutamic acid residues, as required for activity under alkaline conditions. The qualitative nature of these arguments clearly highlights the need to experimentally and theoretically dissect the role of global and local electrostatic interactions in establishing the pK_a values and hence pH optima of enzymes. In closing, we note that the observed trends in the pI values of the family 11 xylanases could simply reflect requirements for stability or solubility in the environmental conditions under which these enzymes have evolved to be active.

Comparison to other glycosidases

A similar triad of carboxylate groups, as present in N35D BCX or acidic xylanases, is seen in other glycosidases. However, in contrast to the family 11 xylanases, a negatively charged aspartic acid residue near the acid/base catalyst is proposed to raise the pH optimum (pH 6.0) (Knegtel *et al*., 1995) of cyclodextrin glycosyl transferases (CGTase) (Klein *et al*., 1992; Strokopytov *et al*., 1995). In *Bacillus circulans* strain 251 CGTase, the nucleophile, Asp229, the acid/base catalyst, Glu257, and the aspartic acid group adjacent to it, Asp328, all occupy a geometrical arrangement very similar to that found in BCX. The interaction between these residues is strong in the unliganded structure (2.7 Å separation between Glu257 $O^{\varepsilon 2}$ and Asp328 $O^{\delta 2}$) and weaker when the substrate is bound (3.6 Å) (Strokopytov *et al*., 1995). In their analysis of *A. niger* xylanase I, Krengel & Dijkstra (1996) suggest a reason for the opposite effect of a negatively charged aspartate near the acid/base catalyst in lowering the pH optimum of xylanases while raising it in the CGTases. Upon substrate binding, Asp328 moves to form a new hydrogen bond with the substrate instead of with Glu257. In this manner, the proton on Glu257 is available for catalysis at higher pH values because it is no longer bound by Asp328 (Krengel & Dijkstra, 1996).

A similar arrangement of catalytic residues is observed in the α-amylases. Functioning at a neutral pH optimum, pig pancreatic α-amylase (PPA) (Qian *et al*., 1994) contains the three residues analogous to those found in both the CGTases (Strokopytov *et al*., 1995) and the acidic family 11 xylanases. In PPA, Glu233 is the proposed acid/base catalyst, with Asp300 adjacent to it, while Asp197 functions as the nucleophile. Asp300 is fully conserved amongst α-amylases (Brayer *et al*., 1995) and, along with a chloride ion (Qian *et al*., 1994) that is situated 4.8 Å away from Glu233 in the unliganded structure (Machius *et al*., 1996), is proposed to play a role in elevating the pK_a of the acid/base catalyst (Glu233). In contrast to the family 11 xylanases, however, the distances between the acid/base catalyst and the adjacent aspartic acid residue are greater in the α-amylases, being 6.2 Å between Glu233 $O^{\varepsilon 2}$ and Asp300 $O^{\delta 2}$ in PPA, and 3.9 Å in human pancreatic α-amylase (HPA) (Brayer *et al*., 1995).

Distinct from PPA and HPA, the acidic α-amylase from *A. niger* exhibits maximal activity at pH ~3-4, yet also contains an adjacent aspartic acid residue, Asp297, 3.8 Å away from the acid/base catalyst, Glu230 (Boel *et al*., 1990). Interestingly, however, fungal α-amylases do not bind chloride ions in the active site, whereas animal α-amylases do (Brayer *et al*., 1995). This may further implicate the evolutionary role of the negatively charged chloride ion in shifting the pH optimum of animal α-amylases to neutral pH by elevating the pK_a of the acid/base catalyst. It remains to be seen, however, if the fungal α-amylases from *A. niger* use the same mechanism as the xylanases in lowering the pH optimum of the enzyme through an aspartic acid residue adjacent to the acid/base catalyst.

Conclusion

The residue at position 35 plays a significant role in determining the pH optima of the family 11 xylanases. Using site-directed mutagenesis, we were able to confirm what was known from nature and modify BCX, an ''alkaline'' xylanase, to function under more acidic conditions without any reduction in its net activity. Counter-intuitively, the presence of an aspartic acid residue adjacent to the acid/base catalyst serves to lower the pH optimum of N35D BCX, instead of raising it as would be predicted from simple electrostatic considerations. Furthermore, we demonstrated with ^{13}C-NMR that Asp35 indeed elevates the pK_a of the acid/base catalyst, Glu172, significantly from 6.7 to 8.4.

To explain this paradox, we propose that N35D BCX, and by inference all ''acidic'' family 11 xylanases, functions using a reverse protonation mechanism. In this catalytic scheme, Asp35 ($pK_a = 3.7$) and Glu172 act together to fulfil the role of the acid/base catalyst, donating a proton to the glycosidic oxygen atom, while Glu78 ($pK_a = 5.7$) still serves as the nucleophile. Only a small percentage of the enzyme (~1 %) is in the requisite ionization state at this optimal pH. However, this form functions as a highly effective catalyst, since a strong hydrogen bond, formed between Asp35 and Glu172 in the glycosyl-enzyme intermediate, substantially stabilizes the transition state for glycosyl transfer. The enzyme becomes inactive at higher pH, since loss of the second proton from the Asp35-Glu172 pair would remove this strong hydrogen bonding interaction and result in substantial charge repulsion between these active-site residues. This study highlights the complexity of possible electrostatic interactions within a protein and the diverse mechanisms by which the pH optima of enzymes can be set.

Materials and Methods

Cloning, mutagenesis and protein expression

The synthetic gene encoding BCX was cloned into the pCW plasmid system under control of an inducible *tac* promoter, as described (McIntosh *et al*., 1996; Sung *et al*., 1993; Wakarchuk *et al*., 1994). To create the genes encoding N35D, N35D/E78Q and N35D/E172Q, site-directed mutagenesis was performed using a QuickChange™ Site-Directed Mutagenesis Kit (Stratagene Cloning Systems, La Jolla, CA). The following oligonucleotide primers were used in the mutagenesis of WT BCX to N35D BCX (based on complementarity to the synthetic BCX gene (Sung *et al*., 1993)): 5′ GG TCT AAT ACT GGG **GAC** TTC GTA GTC GG 3′ and 5′ CC GAC TAC GAA **GTC** CCC AGT ATT AGA CC 3′. The double mutants, N35D/E78Q and N35D/E172Q BCX, were made by performing further site-directed mutagenesis on the N35D BCX gene using the following oligonucleotide primer pairs: for N35D/E78Q, 5′ G CGT TCG CCA CTG ATT **CAA** TAT TAC GTT GTC G 3′ and 5′ C GAC AAC GTA ATA **TTG** AAT CAG TGG CGA ACG C 3′; for N35D/E172Q, 5′ GTA ATG GCG ACC **CAA** GGC TAC CAG AGC 3′ and 5′ GCT CTG GTA GCC **TTG** GGT CGC CAT TAC 3′. All other recombinant DNA procedures, such as plasmid isolation and purification, were performed as recommended by the manufacturers. After the sequences were confirmed by automated DNA sequencing, the mutagenized plasmids were transformed into *Escherichia coli* strain BL21 (λDE3) using electroporation or calcium chloride-heat shock.

Proteins used for kinetic studies were expressed in *E. coli* strain BL21 grown in TYP medium at 37 °C until the time of induction ($A_{600} = 0.5$-0.6) and thereafter at 30 °C until the cells were harvested 16 hours later. Protein expression was induced by addition of IPTG to a final concentration of 0.75 mM. Purification was performed as described, using SP-Sepharose™ ion-exchange chromatography followed by Sephacryl S-100™ HR size-exclusion chromatography (Pharmacia Biotech, Inc.) (Sung *et al*., 1993). Fresh column material was used for different proteins to prevent any possible cross-contamination. Proteins were purified to >95 % homogeneity as judged by SDS-PAGE and Coomassie blue staining. Further characterization was performed using a Perkin Elmer Sciex API III electrospray mass spectrometer with the following results: N35D, observed 20,402(±3.5) Da, expected 20,402 Da; N35D/E78Q, observed 20,400(±3.5) Da, expected 20,401 Da; N35D/E172Q, observed 20,401(±3.5) Da, expected 20,401 Da.

N35D BCX, ^{13}C-enriched in the side-chain δ-carbonyl group of the glutamate and glutamine residues, was expressed as described (McIntosh *et al*., 1996). Bacteria were grown in a synthetic medium (Anderson *et al*., 1993; McIntosh *et al*., 1996; Muchmore *et al*., 1989) containing 275-325 mg/l 99 % L-[δ-^{13}C]glutamate (Tracer Technology, Cambridge, MA). The isotopically labelled proteins were expressed and purified as above, except that the size-exclusion chromatography step was not performed. The [δ-^{13}C]Glu and -Gln-enriched xylanases were purified to >90 % homogeneity as judged by SDS-PAGE and Coomassie blue staining. Further characterization was performed using electrospray mass spectrometry, yielding an observed mass of 20,406(±3.5) Da (expected 20,409 Da) for isotopically labelled N35D BCX. The expected mass value was calculated assuming ~100 % ^{13}C enrichment of seven residues. Deviations from observed and expected molecular masses reflects isotopic dilution of the [δ-^{13}C]glutamate.

Enzyme kinetics

Steady-state kinetics

Several aryl β-xylobiosides were used as substrates in the assays described below: 2,5-dinitrophenyl β-xylobioside (2,5-DNPX_2), $\Delta\varepsilon_{440\ nm,pH6.0} = 3.57\ mM^{-1}\ cm^{-1}$ (where Δε is the difference in molar absorptivity between the phenol and its corresponding xylobioside); 3,4-dinitrophenyl β-xylobioside (3,4-DNPX_2), $\Delta\varepsilon_{400nm,pH6.0} = 11.71\ mM^{-1}\ cm^{-1}$; orthonitrophenyl β-xylobioside (ONPX_2), $\Delta\varepsilon_{400\ nm,pH6.0} = 1.07\ mM^{-1}\ cm^{-1}$; and phenyl β-xylobioside (PhX_2), $\Delta\varepsilon_{288nm,pH12.2} = 2.17\ mM^{-1}\ cm^{-1}$. Inhibition studies were performed using 2,4-dinitrophenyl 2-deoxy-2-fluoro-β-xylobioside (DNP2FXb) as a mechanism-based inhibitor. All substrates and inhibitors were synthesized and characterized according to previously published procedures (Lawson *et al*., 1997; Ziser *et al*., 1995). All other materials, unless otherwise stated, were obtained from the Sigma Chemical Company. Spectrophotometric assays were performed on either a Pye Unicam 8700 or UV4 UV/Vis spectrophotometer, both equipped with a circulating waterbath for temperature control. Assays were carried out in 200 µl micro black-walled quartz cuvets with a 1 cm path-length, as described (Lawson *et al*., 1997). The pH values of assay solutions were measured using a Corning G-P Micro Combo™ electrode. Steady-state kinetic data were fitted using the programs PlotData (TRIUMF, University of British Columbia) and GraFit (Leatherbarrow, 1998).

Assays used to determine the Michaelis-Menten steady-state parameters, k_{cat} and K_m, utilized the appropriate aryl β-xylobioside substrate in 20 mM Mes (pH 6.0), 50 mM NaCl, 0.1 % (w/v) bovine serum albumin. Typically, substrate concentrations were varied from $0.2K_m$ to $5K_m$. After 15 minutes preincubation at 40 °C, 10 µl of enzyme at an appropriate concentration (2.0×10^{-4} mM to 7.0×10^{-2} mM final) was added to 190 µl of the assay solution. The rates of enzymatic

hydrolysis of the aryl β-xylobiosides were determined by monitoring the rate of phenol release at the appropriate wavelength in a continuous assay at 40 °C. Enzyme concentrations and reaction times were chosen such that less than 10 % of the total substrate was hydrolyzed over the course of the measurement. In the case of PhX_2, a stopped assay was used to measure enzymatic hydrolysis rates. After an appropriate time, 600 µl of 200 mM Na_3PO_4 (pH 12.3) buffer was added to terminate the reaction. The absorbance of the released phenol was measured at 288 nm and corrected for both the spontaneous hydrolysis of PhX_2 and the background absorbance of the enzyme. All other conditions were identical with those listed above for assays containing the other aryl β-xylobiosides. Experimental rates measured at each given substrate concentration were fitted to the standard Michaelis-Menten expression to determine the parameters k_{cat} and K_m. Values of k_{cat}/K_m were determined from the slope of a Lineweaver-Burke plot. Brønsted plots (not shown) were constructed by plotting the log of the rate constant against the pK_a of the leaving group, according to the Brønsted equation. The Brønsted coefficient, $\beta_{1\,g}$, was obtained from the slope of the plot determined by a linear least-squares fitting of the data using the program Grafit (Leatherbarrow, 1998).

Assays used to determine the pH-dependence of k_{cat}/K_m employed low concentrations of $ONPX_2$ substrate (0.35 mM), 50 mM NaCl, 0.1 % bovine serum albumin, and the appropriate buffer for a given pH range (pH 2-5: 20 mM succinate; pH 5-7: 20 mM Mes; pH 7-8: 20 mM Hepes; pH 8-11: 20 mM Ches). After 15 minutes preincubation at 25 °C, the enzymatic reaction was initiated by addition of 10 µl of enzyme (3.0×10^{-3} mM final) to 190 µl of the assay solution. Progress curves were followed by measuring the release of *o*-nitrophenolate at 400 nm *versus* time until at least 80 % substrate depletion was observed. The pH of each assay solution was measured after completion of the reaction. An aliquot of the assay mix was then re-assayed at pH 6.0 to confirm the stability of the enzyme compared to an aliquot of unassayed enzyme that had not been exposed to assay conditions. Experimental data were fitted to a pseudo-first-order expression, which upon division by the enzyme concentration yielded k_{cat}/K_m values. This method obviated the need to correct for the variation of extinction coefficient of $ONPX_2$ with pH and eliminated any errors associated with the determination of substrate concentrations. The k_{cat}/K_m data were then plotted as a function of pH and fitted to a bell-shaped activity profile, described in equation (1), from which apparent pK_a values were determined:

$$\left(\frac{k_{cat}}{K_m}\right)_{obs} = \left(\frac{k_{cat}}{K_m}\right)_{max} \left(\frac{1}{1 + \frac{10^{-pH}}{10^{-pK_{a1}}} + \frac{10^{-pK_{a2}}}{10^{-pH}}}\right) \quad (1)$$

Pre-steady-state kinetics

Pre-steady-state kinetic measurements were taken for mutant BCX proteins using a stopped-flow spectrophotometer (Olis RSM-1000) with a 2 cm path-length cell and a circulating waterbath, as described (Zechel *et al.*, 1998). The dead-time of the instrument is 2.5 ms. Data were collected at a rate of 1000 spectra/second over ten seconds. Assays consisted of various amounts of 2,5-$DNPX_2$ substrate (0.30 mM to 2.20 mM) and enzyme (1.0×10^{-3} mM to 2.0×10^{-3} mM) in 10 mM Mes (pH 6.0), 25 mM NaCl at 25 °C. The limited solubility of 2,5-$DNPX_2$ under the conditions described precluded assays containing higher concentrations of substrate. Since no pre-steady-state burst was observed with N35D, N35D/E78Q or N35D/E172Q BCX, further data analysis was not necessary.

Kinetics of inhibition

Inhibition studies of N35D BCX were performed using previously described methods (Miao *et al.*, 1994). Enzyme (1.5×10^{-3} mM) was incubated at 40 °C in a buffer (pH 4.1) containing 20 mM succinate, 50 mM NaCl and 0.1 % bovine serum albumin in the presence of DNP2FXb inhibitor at concentrations of 1.70 mM, 1.00 mM, 0.65 mM or 0.40 mM. A control in which no inhibitor was added was also performed. Residual enzymatic activity was determined by removing 5 µl aliquots of the reaction mixture at various times and assaying in a solution of 2.89 mM $ONPX_2$ in 20 mM Mes (pH 6.0), 20 mM NaCl, 0.1 % bovine serum albumin by monitoring the release of *o*-nitrophenolate at 400 nm. Pseudo-first-order rate constants (k_{obs}) at each inhibitor concentration were determined by fitting the residual activity (v/v_o) *versus* time data directly to a first-order equation as described (Miao *et al.*, 1994). Values of k_i (inhibition rate constant) and K_i (dissociation constant for the inhibitor) were determined by fitting values of k_{obs} to equation (2). The second-order rate constant, k_i/K_i, was determined from the slope of a reciprocal plot:

$$k_{obs} = \frac{k_i[\text{DNP2FXb}]}{K_i + [\text{DNP2FXb}]} \quad (2)$$

NMR

All NMR spectra were recorded using a Varian Unity™ spectrometer operating at 500 MHz for protons.

Titration curves

The [δ-^{13}C]Glu and -Gln-enriched N35D BCX protein was dialyzed or exchanged, using a microconcentration device, into 10 mM sodium phosphate, 10 % ^2H_2O/90 % H_2O, at pH* ~6.0. The sample contained 1.20 mM of selectively labelled N35D BCX in a final volume of 2.0 ml. One-dimensional ^{13}C-NMR spectra were recorded as a function of pH* at 25 °C and processed as described (McIntosh *et al.*, 1996). Chemical shifts were referenced to an external sample of DSS at 0.00 ppm.

The ^{13}C-NMR spectra of [δ-^{13}C]Glu and -Gln-enriched N35D BCX, covalently modified with DNP2FXb, were recorded and processed as described above for the uninhibited protein. Solid DNP2FXb (2.00 mM final) was added directly to the ^{13}C-labelled protein, initially at 1.20 mM in 2.0 ml of 10 mM sodium phosphate, 10 % ^2H_2O/90 % H_2O at pH* 6.21. The protein was completely modified within 30 minutes, as judged by ^{13}C-NMR measurements, and was stable for the period over which the measurements were taken. The inhibition was confirmed by mass spectrometry (observed 20,677(±2) Da, expected 20,675 Da).

Titration curves were generated by recording ^{13}C-NMR spectra of [δ-^{13}C]Glu and -Gln-labelled xylanases as a function of pH* at 25 °C. Proteins were titrated

using microliter aliquots of either 0.25-0.50 M HCl or NaOH. The pH* of the sample was determined using a Corning G-P Micro Combo™ electrode. After measuring the acidic limb of the titration curve, the protein was exchanged into neutral buffer, using a micro concentrating device, to remove any excess salt and to avoid aggregation resulting from the addition of a large quantity of base. Titration of the basic limb was then carried out in a manner similar to that used for the acidic limb. The sample was centrifuged periodically to remove any precipitate that formed during the titration. Individual δ-carbon resonances of glutamate and glutamine side-chains of mutant xylanase proteins were assigned on the basis of previous analysis of the WT spectra (McIntosh *et al*., 1996; Plesniak *et al*., 1996b). pK_a values were determined by non-linear least-squares fitting of the observed data to models involving one, two, or three sequential ionizations (equations (3)-(5)) (Shrager *et al*., 1972) using the program PlotData (TRIUMF, University of British Columbia). The inherent error of the pH measurements is estimated to be ±0.1 pH unit.

NMR-derived titration curves characterized by one, two, or three apparent pK_a values are described by equation (3), (4), and (5), respectively. δ_{obs} is the chemical shift of the residue being monitored, and δ_i represents the chemical shift of the residue in each ionization state of the enzyme:

$$\delta_{obs} = \frac{\delta_a 10^{-pH} + \delta_b 10^{-pK_a}}{10^{-pH} + 10^{-pK_a}} \quad (3)$$

$$\delta_{obs} = \frac{\delta_a 10^{-2pH} + \delta_b 10^{-(pH+pK_{a1})} + \delta_c 10^{-(pK_{a1}+pK_{a2})}}{10^{-2pH} + 10^{-(pH+pK_{a1}} + 10^{-(pK_{a1}+pK_{a2})}} \quad (4)$$

$$\delta_{obs} = \frac{\begin{array}{c}\delta_a 10^{-(3pH)} + \delta_b 10^{-(pK_{a3}+2pH)} \\ +\delta_c 10^{-(pK_{a2}+pK_{a3}+pH)} + \delta_d 10^{-(pK_{a1}+pK_{a2}+pH_{a3})}\end{array}}{\begin{array}{c}10^{-(3pH)} + 10^{-(pK_{a3}+2pH)} + 10^{-(pK_{a2}+pK_{a3}+pH} \\ +10^{-(pK_{a1}+pK_{a2}+pK_{a3})}\end{array}} \quad (5)$$

Selection of the appropriate model was based on the criterion of using the minimal number of ionization events to adequately fit the observed titration data.

Deuterium isotope shifts

Deuterium isotope shifts of the [δ-^{13}C]Glu and -Gln side-chains of isotopically labelled N35D BCX were measured for both free and inhibited proteins. Spectra were recorded at 25 °C and processed as described above. The initial sample conditions for the free protein were 10 mM sodium phosphate, 10 % ^2H_2O at pH* 6.32, 0.72 mM N35D, while for the inhibited protein the initial conditions were 10 mM sodium phosphate, 10 % ^2H_2O at pH* 5.90, 1.20 mM N35D. After recording the initial spectra of these proteins in 10 % ^2H_2O, samples were exchanged into 90 % ^2H_2O using a microconcentration device, and the pH* was readjusted to the same value as in the respective 10 % ^2H_2O sample by addition of 0.1 M HCl.

Stereochemistry

The stereochemical course of hydrolysis of N35D BCX was determined by adding 60 μl of enzyme (0.015 mM N35D final) directly to a 5 mm NMR tube containing 5.4 mM $ONPX_2$, 10 mM sodium phosphate, 50 mM NaCl, 99.9 % ^2H_2O at pH* 4.8 (Lawson *et al*., 1996). One-dimensional ^{1}H spectra were recorded at 25 °C as a function of time ($t = 5$, 10, 20, 25, 210 minutes) after addition of enzyme in order to monitor the hydrolysis and subsequent mutarotation of the anomeric proton of the xylobiose unit proximal to the departing phenolate group.

Electrospray mass spectrometry

Labelling and identification of the active-site nucleophile was performed as described (Lawson *et al*., 1996; Miao *et al*., 1994). N35D BCX (0.50 mM final) was inhibited at 40 °C in a buffer (pH 4.1) containing 20 mM succinate, 50 mM NaCl, and DNPX2FXb (1.50 mM final). After eight hours of inhibition, an aliquot of the inhibited sample was analyzed using a Perkin Elmer Sciex API III LC-ESMS system. A major peak corresponding to the mass of the covalently labelled protein was observed (20,666(±2) Da) and a relatively minor peak corresponding to the mass of the unlabelled protein were observed (20,401(±2) Da). After heat-denaturing by boiling in a waterbath for two minutes and subsequent cooling to room temperature, the covalently modified N35D protein (0.1 mM final) was subject to proteolytic digestion for seven hours using a solution containing 0.5 mg/ml pepsin and 200 mM sodium phosphate (pH 2.0). A control experiment in which no DNP2FXb inhibitor was added was performed in parallel. Neutral loss MS/MS studies on the labelled peptide were performed as described for WT BCX (Miao *et al*., 1994). The triple quadrupole neutral loss scan mode was set to detect a mass loss of m/z 133.5, corresponding to the loss of 2FXb from a peptide ion in the doubly charged state.

X-ray crystallography

Crystals of N35D BCX were grown and soaked with DNP2FXb at pH 7.5 as described for the WT enzyme (Sidhu *et al*., 1999). Diffraction data were collected from a single N35D BCX crystal and a single crystal of N35D-2FXb BCX on a Rigaku R-AXIS IIC imaging plate area detector system using CuK_α radiation supplied by a Rigaku RU300 rotating anode generator operating at 50 kV and 100 mA. Each diffraction data frame was exposed for 20 minutes, during which time the crystal was oscillated through 1.2 °. Intensity data were integrated, scaled, and reduced to structure factor amplitudes with the HKL suite of programs (Otwinowski & Minor, 1997). Because both types of crystals retained unit cells isomorphous to WT BCX, the WT model, with residue 35 truncated to alanine was used as the starting model in each case. These models were subjected to rigid body, simulated annealing, positional, and individual isotropic thermal factor refinement using X-PLOR (Brünger, 1992) and the CCP4 Suite (Collaborative Computational Project Number 4, 1994). At this point $F_o - F_c$ difference electron density maps were calculated and both Asp35 and the 2FXb saccharide were built into observed density with the program O (Jones *et al*., 1991). The models were then refined further with X-PLOR. A standard carbohydrate topology and parameter library was used in the refinement of the glycosyl-enzyme intermediate (Sidhu *et al*., 1999). The structural models were examined periodically during refinement with $F_o - F_c$, $2F_o - F_c$, and fragment-deleted difference electron density maps. Manual adjustments were made as necessary and solvent molecules were identified. The validity of solvent

molecules was assessed based on both hydrogen bonding potential to appropriate protein atoms and refinement of a thermal factor of less than 75 $Å^2$. The coordinate error estimated from a Luzzati plot (Luzzati, 1952) is 0.18 Å for N35D BCX and 0.19 Å for N35D-2FXb BCX. Structural illustrations using atomic coordinates were generated using the programs Bobscript (Kraulis, 1991) and Raster3D (Merrit & Murphy, 1994).

Protein Data Bank accession codes

Atomic coordinates and related structure factors have been deposited in the RCSB Protein Data Bank (Bernstein *et al*., 1977) with identification codes 1C5H for N35D BCX and 1C5I for N35D-2FXb BCX.

Acknowledgments

We thank Dr Shouming He and Lloyd Mackenzie for assistance with the ESMS studies, Timothy Hiebert for synthesizing various substrates, Nham Nguyen for crystallographic assistance and Drs Gideon Davies, Warren Wakarchuk, and Tony Warren for helpful discussions throughout this project. This work was funded by the Government of Canada's Network of Centres of Excellence Program supported by the Medical Research Council of Canada and the Natural Sciences and Engineering Research Council through PENCE Inc. L.P.M. acknowledges the Alexander von Humbolt-Stiftung for a Research Fellowship.

References

Anderson, D. E., Lu, J., McIntosh, L. P. & Dahlquist, F. W. (1993). *The Folding, Stability and Dynamics of T4 Lysozyme: A Perspective Using Nuclear Magnetic Resonance* (Clore, G. M. & Gronenborn, A. M., eds), McMillian Press, London.

Bernstein, F. C., Koetzle, T. F., Williams, G. J., Meyer, E. E., Jr, Brice, M. D., Rodgers, J. R., Kennard, O., Shimanouchi, T. & Tasumi, M. (1977). The Protein Data Bank: a computer-based archival file for macromolecular structures. *J. Mol. Biol.* **112**, 535-542.

Birsan, C., Johnson, P., Joshi, M., MacLeod, A., McIntosh, L., Monem, V., Nitz, M., Rose, D. R., Tull, D., Wakarchuck, W. W., Wang, Q., Warren, R. A., White, A. & Withers, S. G. (1998). Mechanisms of cellulases and xylanases. *Biochem. Soc. Trans.* **26**, 156-160.

Boel, E., Brady, L., Brzozowski, A. M., Derewenda, Z., Dodson, G. G., Jensen, V. J., Peterson, S. B., Swift, H., Thim, L. & Woldike, H. F. (1990). Calcium binding in α-amylases: an X-ray diffraction study at 2.1 Å resolution of two enzymes from *Aspergillus*. *Biochemistry*, **29**, 6244-6249.

Brayer, G. D., Luo, Y. & Withers, S. G. (1995). The structure of human pancreatic alpha-amylase at 1.8 Å resolution and comparisons with related enzymes. *Protein Sci.* **4**, 1730-1742.

Brünger, A. T. (1992). *X-PLOR Version 3.1: A System for X-ray Crystallography and NMR*, Yale University Press, New Haven, CT.

Cleland, W. W., Frey, P. A. & Gerlt, J. A. (1998). The low barrier hydrogen bond in enzymatic catalysis. *J. Biol. Chem.* **273**, 25529-25532.

Collaborative Computational Project Number 4 (1994). The CCP4 suite: programs for protein crystallography. *Acta Crystallog. sect. D*, **50**, 760-763.

Connelly, G. P., Withers, S. G. & McIntosh, L. P. (2000). Analysis of the dynamic properties of *Bacillus circulans* xylanase upon formation of a covalent glycosyl-enzyme intermediate. *Protein Sci.* **9**, 512-524.

Fushinobu, S., Ito, K., Konno, M., Wakagi, T. & Matsuzawa, H. (1998). Crystallographic and mutational analyses of an extremely acidophilic and acid-stable xylanase: biased distribution of acidic residues and importance of Asp37 for catalysis at low pH. *Protein Eng.* **11**, 1121-1128.

Gebler, J., Gilkes, N. R., Claeyssens, M., Wilson, D. B., Beguin, P., Wakarchuk, W. W., Kilburn, D. G., Miller, R. C., Jr, Warren, R. A. & Withers, S. G. (1992). Stereoselective hydrolysis catalyzed by related beta-1,4-glucanases and beta-1,4-xylanases. *J. Biol. Chem.* **267**, 12559-12561.

Gilkes, N. R., Henrissat, B., Kilburn, D. G., Miller, R. C., Jr & Warren, R. A. (1991). Domains in microbial beta-1,4-glycanases: sequence conservation, function, and enzyme families. *Microbiol. Rev.* **55**, 303-315.

Gruber, K., Klintschar, G., Hayn, M., Schlacher, A., Steiner, W. & Kratky, C. (1998). Thermophilic xylanase from *Thermomyces lanuginosus*: high-resolution X-ray structure and modeling studies. *Biochemistry*, **37**, 13475-13485.

Jones, T. A., Zhou, J. Y., Cowan, S. W. & Kjeldgaard, M. (1991). Improved methods for building protein molecules in electron density maps and the location of errors in these maps. *Acta Crystallog. sect. A*, **47**, 110-119.

Joshi, M. D., Hedberg, A. & McIntosh, L. P. (1997). Complete measurement of the pKa values of the carboxyl and imidazole groups in *Bacillus circulans* xylanase. *Protein Sci.* **6**, 2667-2670.

Karplus, P. A., Pearson, M. A. & Hausinger, R. P. (1997). 70 Years of crystalline urease: what have we learned? *Acc. Chem. Res.* **30**, 330-337.

Kirby, A. J. (1997). Efficiency of proton transfer catalysis in models and enzymes. *Acc. Chem. Res.* **30**, 290-296.

Klein, C., Hollender, J., Bender, H. & Schulz, G. E. (1992). Catalytic center of cyclodextrin glycosyltransferase derived from X-ray structure analysis combined with site-directed mutagenesis. *Biochemistry*, **31**, 8740-8746.

Knegtel, R. M. A., Strokopytov, B., Penninga, D., Faber, O. G., Rozeboom, H. J., Kalk, K. H., Dijkhuizen, L. & Dijkstra, B. W. (1995). Crystallographic studies of the interaction of cyclodextrin glycosyltransferase from *Bacillus circulans* strain 251 with natural substrates and products. *J. Biol. Chem.* **270**, 29256-29264.

Koshland, D. E. (1953). Stereochemistry and mechanism of enzymatic reactions. *Biol. Rev.* **28**, 416-436.

Kraulis, P. J. (1991). MOLSCRIPT: a program to produce both detailed and schematic plots of proteinstructures. *J. Appl. Crystallog.* **24**, 946-950.

Krengel, U. & Dijkstra, B. W. (1996). Three-dimensional structure of endo-1,4-beta-xylanase I from *Aspergillus niger*: molecular basis for its low pH optimum. *J. Mol. Biol.* **263**, 70-78.

Ladner, H. K., Led, J. J. & Grant, D. M. (1975). Deuterium isotope effects on ^{13}C chemical shifts in amino acids and dipeptides. *J. Magn. Reson.* **20**, 530-534.

Lawson, S. L., Wakarchuk, W. W. & Withers, S. G. (1996). Effects of both shortening and lengthening

the active site nucleophile of *Bacillus circulans* xylanase on catalytic activity. *Biochemistry,* **35**, 10110-10118.

Lawson, S. L., Wakarchuk, W. W. & Withers, S. G. (1997). Positioning the acid/base catalyst in a glycosidase: studies with *Bacillus circulans* xylanase. *Biochemistry,* **36**, 2257-2265.

Leatherbarrow, R. J. (1998). *Gra-Fit, Version 4.0*, Erithacus Software Ltd., UK, Staines.

Luzzati, P. V. (1952). Traitment statistique des erreurs dans la determination des structures cristallines. *Acta Crystallog. sect. A,* **50**, 803-810.

Machius, M., Vertesy, L., Huber, R. & Wiegand, G. (1996). Carbohydrate and protein-based inhibitors of porcine pancreatic α-amylase: structure analysis and comparison of their binding characteristics. *J. Mol. Biol.* **260**, 409-421.

McDaniel, D. H. & Brown, H. C. (1953). Hydrogen bonding as a factor in the ionization of dicarboxylic acids. *Science,* **118**, 370-372.

McIntosh, L. P., Hand, G., Johnson, P. E., Joshi, M. D., Korner, M., Plesniak, L. A., Ziser, L., Wakarchuk, W. W. & Withers, S. G. (1996). The pK_a of the general acid/base carboxyl group of a glycosidase cycles during catalysis: a ^{13}C-NMR study of *Bacillus circulans* xylanase. *Biochemistry,* **35**, 9958-9966.

Merrit, E. A. & Murphy, M. E. (1994). Raster3D version 2.0: a program for photorealistic molecular graphics. *Acta Crystallog. sect. D,* **50**, 869-873.

Miao, S., Ziser, L., Aebersold, R. & Withers, S. G. (1994). Identification of glutamic acid 78 as the active site nucleophile in *Bacillus subtilis* xylanase using electrospray tandem mass spectrometry. *Biochemistry,* **33**, 7027-7032.

Mock, W. L. & Aksamawati, M. (1994). Binding to thermolysin of phenolate-containing inhibitors necessitates a revised mechanism of catalysis. *Biochem. J.* **302**, 57-68.

Mock, W. L. & Stanford, D. J. (1996). Arazoformyl dipeptide substrates for thermolysin. confirmation of a reverse protonation catalytic mechanism. *Biochemistry,* **35**, 7369-7377.

Muchmore, D. C., McIntosh, L. P., Russell, C. B., Anderson, D. E. & Dahlquist, F. W. (1989). Expression and nitrogen-15 labeling of proteins for proton and nitrogen-15 nuclear magnetic resonance. *Methods Enzymol.* **177**, 44-73.

Otwinowski, Z. & Minor, W. (1997). Processing of X-ray diffraction data collected in oscillation mode. *Methods Enzymol.* **276**, 307-326.

Plesniak, L. A., Connelly, G. P., Wakarchuk, W. W. & McIntosh, L. P. (1996a). Characterization of a buried neutral histidine residue in *Bacillus circulans* xylanase: NMR assignments, pH titration, and hydrogen exchange. *Protein Sci.* **5**, 2319-2328.

Plesniak, L. A., Wakarchuk, W. W. & McIntosh, L. P. (1996b). Secondary structure and NMR assignments of *Bacillus circulans* xylanase. *Protein Sci.* **5**, 1118-1135.

Qian, M., Haser, R., Buisson, G., Duee, E. & Payan, F. (1994). The active center of a mammalian α-amylase. Structure of the complex of a pancreatic α-amylase with a carbohydrate inhibitor refined to 2.2 Å resolution. *Biochemistry,* **33**, 6284-6294.

Richard, J. P. (1998). The enhancement of enzymatic rate accelerations by Brønsted acid-base catalysis. *Biochemistry,* **37**, 4305-4309.

Sabini, E., Sulzenbacher, G., Dauter, M., Dauter, Z., Jorgensen, P. L., Schulein, M., Dupont, C., Davies, G. J. & Wilson, K. S. (1999). Catalysis and specificity in enzymatic glycoside hydrolysis: a ^{2,5}B conformation for the glycosyl-enzyme intermediate revealed by the structure of the *Bacillus agaradhaerens* family 11 xylanase. *Chem. Biol.* **6**, 483-492.

Shrager, R. I., Cohen, J. S., Heller, S. R., Sachs, D. H. & Schechter, A. N. (1972). Mathematical models for interacting groups in nuclear magnetic resonance titration curves. *Biochemistry,* **11**, 541-547.

Sidhu, G., Withers, S. G., Nguyen, N. T., McIntosh, L. P., Ziser, L. & Brayer, G. D. (1999). Sugar ring distortion in the glycosyl-enzyme intermediate of a family G/11 xylanase. *Biochemistry,* **38**, 5346-5354.

Sinnot, M. L. (1990). Catalytic mechanisms of enzymic glycosyl transfer. *Chem. Rev.* **90**, 1171-1202.

Strokopytov, B., Penninga, D., Rozeboom, H. J., Kalk, K. H., Dijkhuizen, L. & Dijkstra, B. W. (1995). X-ray structure of cyclodextrin glycosyltransferase complexed with acarbose. Implications for the catalytic mechanism of glycosidases. *Biochemistry,* **34**, 2234-2240.

Sung, W. L., Luk, C. K., Zahab, D. M. & Wakarchuk, W. (1993). Overexpression of the *Bacillus subtilis* and *circulans* xylanases in *Escherichia coli*. *Protein Expr. Purif.* **4**, 200-206.

Torronen, A. & Rouvinen, J. (1995). Structural comparison of two major endo-1,4-xylanases from *Trichoderma reesei*. *Biochemistry,* **34**, 847-856.

Torronen, A. & Rouvinen, J. (1997). Structural and functional properties of low molecular weight endo-1,4-beta-xylanases. *J. Biotechnol.* **57**, 137-149.

Torronen, A., Kubicek, C. P. & Henrissat, B. (1993). Amino acid sequence similarities between low molecular weight endo-1,4-beta-xylanases and family H cellulases revealed by clustering analysis. *FEBS Letters,* **321**, 135-139.

Torronen, A., Harkki, A. & Rouvinen, J. (1994). Three-dimensional structure of endo-1,4-beta-xylanase II from *Trichoderma reesei*: two conformational states in the active site. *EMBO J.* **13**, 2493-2501.

Tull, D. & Withers, S. G. (1994). Mechanisms of cellulases and xylanases: a detailed kinetic study of the exo-beta-1,4-glycanase from *Cellulomonas fimi*. *Biochemistry,* **33**, 6363-6370.

Turnbull, J. L., Waldrop, G. L. & Schachman, H. K. (1992). Ionization of amino acid residues involved in the catalytic mechanism of aspartate transcarbamoylase. *Biochemistry,* **31**, 1285-1294.

Wakarchuk, W., Methot, N., Lanthier, P., Sung, W., Seligy, V., Yaguchi, M., To, R., Campbell, R. & Rose, D. (1992). The 20 kDa xylanase of *Bacillus subtilis*: a structure/function analysis. In *Xylan and Xylanases* (Visor, J., *et al.*, eds), pp. 439-442, Elsevier Science B. V., Amsterdam.

Wakarchuk, W. W., Campbell, R. L., Sung, W. L., Davoodi, J. & Yaguchi, M. (1994). Mutational and crystallographic analyses of the active site residues of the *Bacillus circulans* xylanase. *Protein Sci.* **3**, 467-475.

Wilkins, M. R., Gasteiger, E., Bairoch, A., Sanchez, J. C., Williams, K. L., Appel, R. D. & Hochstrasser, D. F. (1998). Protein identification and analysis tools in the ExPASy server. In *2-D Proteome Analysis Protocols* (Link, A. J., ed.), Humana Press, New Jersey.

Yamazaki, T., Nicholson, L. K., Torchia, D. A., Wingfield, P., Stahl, S. J., Kaufman, J. D., Eyermann, C. J., Hodge, C. N., Lam, P. Y. S., Ru, Y., Jadhav, P. K., Chang, C. & Weber, P. C. (1994).

NMR and X-ray evidence that the HIV protease catalytic aspartyl groups are protonated in the complex formed by the protease and a non-peptide cyclic urea-based inhibitor. *J. Am. Chem. Soc.* **116**, 10791-10792.

Zechel, D. L., Konermann, L., Withers, S. G. & Douglas, D. J. (1998). Pre-steady state kinetic analysis of an enzymatic reaction monitored by time-resolved electrospray ionization mass spectrometry. *Biochemistry,* **37**, 7664-7669.

Ziser, L., Setyawati, I. & Withers, S. G. (1995). Syntheses and testing of substrates and mechanism-based inactivators for xylanases. *Carbohydr. Res.* **274**, 137-153.

Edited by M. F. Summers

(Received 9 December 1999; received in revised form 23 March 2000; accepted 24 March 2000)